Journal of Structural Geology 139 (2020) 104126

Contents lists available at ScienceDirect

Journal of Structural Geology

journal homepage: http://www.elsevier.com/locate/jsg

# Structural evolution of the eastern segment of the Irtysh Shear Zone: Implications for the collision between the East Junggar Terrane and the Chinese Altai Orogen (northwestern China)

Wanwan Hu [a,b], Pengfei Li [a,*], Gideon Rosenbaum [c], Junlai Liu [d], Fred Jourdan [e], Yingde Jiang [a], Dan Wu [f], Jian Zhang [g], Chao Yuan [a], Min Sun [h]

[a] State Key Laboratory of Isotope Geochemistry, Guangzhou Institute of Geochemistry, Chinese Academy of Sciences, Guangzhou, 510640, China
[b] University of Chinese Academy of Sciences, Beijing, 100049, China
[c] School of Earth and Environmental Sciences, The University of Queensland, Brisbane, 4072, Queensland, Australia
[d] State Key Laboratory of Geological Processes and Mineral Resources, China University of Geosciences, Beijing, 100083, China
[e] Western Australian Argon Isotope Facility, JdL Center & School of Earth and Planetary Sciences, Curtin University, Perth, Western Australia, 6845, Australia
[f] CAS Key Laboratory of Mineralogy and Metallogeny, Guangzhou Institute of Geochemistry, Chinese Academy of Sciences, Guangzhou, 510640, China
[g] School of Earth Science and Engineering, Sun Yat-sen University, Guangzhou, 510275, China
[h] Department of Earth Sciences, The University of Hong Kong, Pokfulam Road, Hong Kong, China

ARTICLE INFO

*Keywords:*
Chinese Altai
Central Asian orogenic belt
East Junggar
Irtysh Shear Zone
Transpressional deformation
Accretionary orogen

ABSTRACT

The tectonic evolution of the Central Asian Orogenic Belt (CAOB) involved multiple episodes of arc accretions/collisions, but the reconstruction of these tectonic processes remains relatively poorly constrained. Evidence for a collision between the intra-oceanic island arc system of the East Junggar Terrane and the active margin of the Siberian Craton (Chinese Altai Orogen) is recorded in the eastern segment of the Irtysh Shear Zone (northwestern China). Field observations from the Qinghe area show that this segment of the Irtysh Shear Zone consists of four NW–SE sinistral mylonitic zones, and domains bounded by these mylonitic zones show variable fold patterns. In the northern part of the Irtysh Shear Zone (southern Chinese Altai Orogen), three generations of structures ($D_{CA1}$–$D_{CA3}$) are recognized. The earliest generation of foliation ($S_{CA1}$) is only recognized locally and is transposed to the orientation of the dominant $D_{CA2}$ foliation ($S_{CA2}$). The latter is associated with a shallowly plunging stretching lineation, which is sub-parallel to the NW–SE hinge of $D_{CA3}$ folds. These third-generation folds ($D_{CA3}$) show a steeply-dipping axial plane trending NW–SE. In the southern part of the Irtysh Shear Zone (northern East Junggar Terrane), the structural pattern is simpler and only involves a single generation of penetrative foliation ($S_{EJ1}$). New U–Pb detrital zircon and $^{40}Ar/^{39}Ar$ data provide constraints on the timing of collision and deformation. These results suggest that the collision occurred after the Early Carboniferous, with the timing of sinistral shearing constrained to the Early–Middle Permian. The combination of sinistral shearing and NW–SE $D_{CA3}$ folds likely represents an episode of transpressional deformation, which was driven by oblique collision between the East Junggar Terrane and the Chinese Altai Orogen during the Early–Middle Permian. The occurrence of original sub-horizontal $S_{CA2}$ foliation and associated orogen-parallel stretching lineation might indicate that following the initial collision (after the Early Carboniferous), the southern Chinese Altai Orogen was subjected to orogen-parallel extension. In a larger-scale context, sinistral kinematics along the Irtysh Shear Zone in northwestern China and northeastern Kazakhstan, together with coeval dextral strike-slip deformation farther south, might reflect an eastward escape of orogenic materials, possibly in response to the Permian convergence of the Siberian, Baltic, and Tarim cratons.

## 1. Introduction

The development of the Central Asian Orogenic Belt (CAOB), from the late Precambrian to the late Paleozoic, involved the juxtaposition of multiple microcontinents, magmatic arcs, seamounts, and ophiolitic complexes (Jahn, 2004; Windley et al., 2007; Wilhem et al., 2012; Xiao

* Corresponding author.
*E-mail addresses:* pengfeili@gig.ac.cn, pengfeili2013@gmail.com (P. Li).

https://doi.org/10.1016/j.jsg.2020.104126
Received 27 April 2020; Received in revised form 21 June 2020; Accepted 21 June 2020
Available online 15 July 2020

et al., 2015; Li et al., 2019). Numerous models have been proposed to explain the tectonic evolution of the CAOB. Earlier models by Şengör et al. (1993) and Şengör and Natal'in (1996) have considered a single arc system that was affected by a series of large-scale strike-slip faults. More recent models, however, are based on the assumption that multiple arc systems had operated prior to their final amalgamation within the CAOB (Xiao et al., 2004, 2010; Windley et al., 2007). Understanding when and how these arc systems collided is crucial for tectonic reconstructions.

The Irtysh (Erqis)-Char shear zones represent a major suture within the CAOB, separating the peri-Siberian orogenic system in the north from the Kazakhstan orogenic system and the East Junggar Terrane in the south (Fig. 1a and b; Şengör et al., 1993; Buslov et al., 2004b; Xiao et al., 2010; Li et al., 2015). In northeastern Kazakhstan, three sinistral shear zones (North-East, Irtysh, Char; Fig. 1a) trend NW–SE, with the Char Shear Zone representing the boundary between the peri-Siberian and Kazakhstan orogenic systems (Buslov et al., 2004b; Safonova, 2014; Safonova et al., 2018). In northwestern China, the North-East and Char shear zones merge into the Irtysh Shear Zone, which marks the boundary of the Chinese Altai Orogen (southern segment of the peri-Siberian orogenic system in northwestern China) with the island arc systems of the West Junggar (part of the Kazakhstan orogenic system) and East Junggar terranes (Fig. 1a and b; He et al., 1990; Qu and Zhang, 1991, 1994; Windley et al., 2002; Xiao et al., 2004; Li et al., 2015, 2017; Hong et al., 2017). During the late Paleozoic, the Ob-Zaisan Ocean (also termed the Irtysh Ocean; Xiao et al., 2008), which was located between the peri-Siberian orogenic system and the Kazakhstan orogenic system/the East Junggar Terrane, was progressively consumed by continuous subduction (Cai et al., 2012a; Tong et al., 2012; Li et al., 2015, 2017; Hong et al., 2017; Zhang et al., 2018). The exact timing of this ocean closure is a matter of debate. Closure of the western Ob-Zaisan Ocean, which separated the Chinese Altai Orogen from the West Junngar Terrane in northwestern China (Fig. 1), has been suggested to occur during the latest Carboniferous, based on the recognition of subduction-related magmatism as young as ~313 Ma (Cai et al., 2012a). Final closure of the eastern sector of the Ob-Zaisan Ocean, which separated the Chinese Altai Orogen from the East Junggar Terrane, has been suggested to occur during the earliest Carboniferous (Tong et al., 2012; Hong et al., 2017), Late Carboniferous (Zhang et al., 2018), or Permian (Wan et al., 2013). These conflicting interpretations are based predominantly on geochemical characteristics of igneous rocks from the Chinese Altai Orogen. Based on detrital zircon data, it has been shown that during the Late Carboniferous, there was no exchange of detritus between the East Junggar Terrane and the Chinese Altai Orogen (in the Fuyun area; Fig. 1b), thus supporting the existence of an oceanic basin in this area at that time (Li et al., 2017). However, the lack of constraints from other areas along the suture zone casts doubt on whether other sectors of the oceanic basin had been closed earlier (i.e., diachronous closure along strike), thus calling for further investigation.

The collision between the Chinese Altai Orogen and the East Junggar Terrane is relatively poorly understood. Previous structural studies in the Fuyun area (Fig. 1b) have shown that the collisional front of the Irtysh Shear Zone was subjected to sinistral shearing, thus raising the possibility of oblique collision (Qu and Zhang, 1991, 1994; Laurent-Charvet et al., 2003; Li et al., 2015, 2016a; 2017). The timing of sinistral shearing has been constrained to post-283 Ma on a basis of $^{40}Ar/^{39}Ar$ ages of syn-shearing minerals (Li et al., 2017 and references therein), meaning that oblique convergence might characterize one stage of the collisional history. However, the earlier history of collision, for example, during the latest Carboniferous and earliest Permian, remains poorly understood. Li et al. (2015) inferred that two generations of structures in the Fuyun area (Fig. 1b) were developed prior to sinistral shearing. These findings suggest that prior to oblique convergence, the collisional zone was likely subjected to orogenic thickening and collapse (Li et al., 2015). Such structural observations and interpretations in the Fuyun area are not compatible with structural interpretations from the Qinghe area, farther east (Fig. 1b), where the Irtysh Shear Zone has been interpreted to represent a coaxial deformation zone (Hong et al. (2015). In fact, both sinistral and dextral shearing structures were reported from the Qinghe area (Qu and Zhang, 1991; Laurent-Charvet et al., 2002; Liu et al., 2013). Therefore, it is necessary to re-evaluate the structural evolution of the Qinghe segment of the Irtysh Shear Zone, particularly in the context of the relationships between pure shear and simple shear deformation. Combining such information with the deformation history of the Fuyun area will provide a comprehensive understanding of the collisional processes between the East Junggar Terrane and the Chinese Altai Orogen.

In this paper, we present new structural data from the Qinghe area, in the eastern segment of the Irtysh Shear Zone (Fig. 1b). These data are analyzed in combination with new zircon U–Pb and mica $^{40}Ar/^{39}Ar$ results. Our results provide new constraints on the timing and style of the collision between the East Junggar Terrane and the Chinese Altai Orogen. The results are further discussed in the larger-scale context of the Irtysh Shear Zone in northwestern China and northeastern Kazakhstan, and we highlight the crucial role of large-scale shear zones in the late Paleozoic evolution of the CAOB.

## 2. Geological setting

The NW–SE Irtysh Shear Zone extends from northeastern Kazakhstan, through northwestern China, to western Mongolia (Windley et al., 2002). Structural data from northwestern China (Fuyun area; Fig. 1b) show that the shear zone is characterized by a number of fold zones bounded by sinistral (strike-slip) mylonitic zones (Qu and Zhang, 1991; Li et al., 2015, 2017). One of these mylonitic zones (commonly referred to as the Irtysh Fault; Fig. 1b) separates the Chinese Altai Orogen from the East Junggar Terrane (Qu and Zhang, 1991, 1994; Li et al., 2015, 2017). The Irtysh Fault is cut by the ~N–S Fuyun Fault, which is a Cenozoic dextral fault (Fig. 1b). The Mayin'erbo Fault, to the east of the Fuyun Fault, possibly represents the eastern extension of the Irtysh Fault (Fig. 1b; BGMRX, 1972; Qu and Zhang, 1991, 1994).

The Chinese Altai Orogen represents a southern segment of the peri-Siberian orogenic system that was developed along the margin of the Siberian Craton (Fig. 1a; Windley et al., 2002). The Chinese Altai Orogen can be divided into four tectono-stratigraphic domains: Northern Altai, Central Altai, Qiongkuer, and Southern Altai (Fig. 1b; He et al., 1990; Windley et al., 2002; Xiao et al., 2004). The Northern Altai Domain comprises predominantly Late Devonian to Early Carboniferous meta-volcanic and meta-sedimentary rocks (Windley et al., 2002; Xiao et al., 2004). It is separated from the Central Altai Domain by a north-dipping normal fault (Fig. 1b). The Central Altai Domain, which is the most extensive part of the Chinese Altai Orogen, is dominated by Cambrian to Silurian turbidites and pyroclastic rocks (Habahe Group) and Silurian metasedimentary rocks (Kulumuti Group) that mostly metamorphosed under greenschist to amphibolite facies (Zhuang, 1994; Windley et al., 2002; Long et al., 2007, 2008; Jiang et al., 2015). The Qiongkuer Domain comprises mainly Devonian meta-volcanic/sedimentary rocks (Kangbutiebao and Altai formations), which are considered to be equivalent to the Mayin'erbo Formation in the Qinghe area (Fig. 1b; BGMRX, 1972). The Southern Altai Domain, which is the southernmost part of the Chinese Altai Orogen, includes the so-called Irtysh Complex, which consists of schist, gneiss, amphibolite, migmatite, quartzite, and metachert (Briggs et al., 2007; Xiao et al., 2009). Previous studies have suggested that the Irtysh Complex represents an accretionary complex associated with northeastward subduction (present coordinates) of the Ob-Zaisan oceanic plate (Ohara et al., 1997; Xiao et al., 2009; Chen et al., 2019). The Paleozoic volcano-sedimentary rocks of the Chinese Altai Orogen are intruded by widespread granitic plutons, which show two age peaks of ~400 Ma and ~280 Ma (Wang et al., 2010, 2014a; Cai et al., 2012a; Tong et al., 2014b).

The East Junngar Terrane, which is separated from the West Junggar

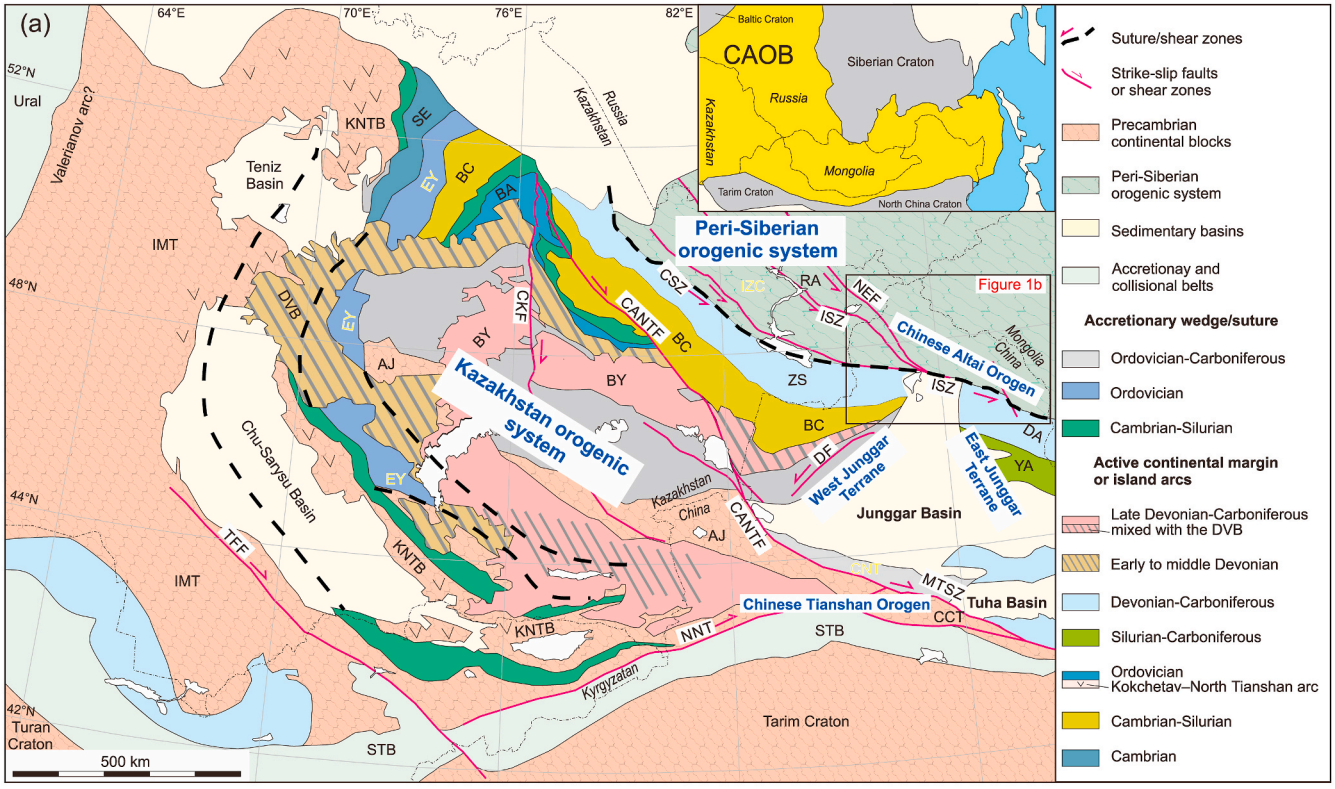


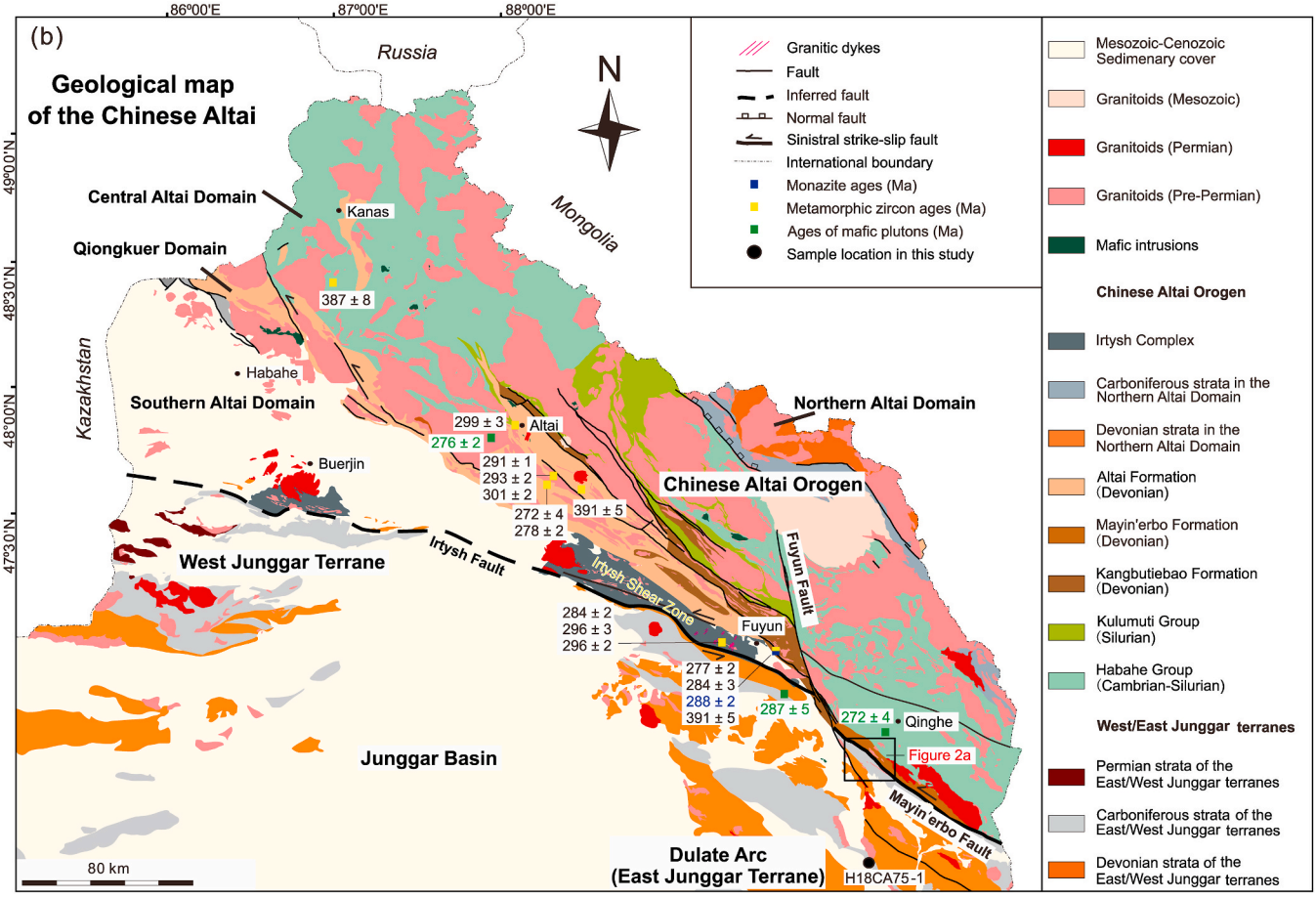


*(caption on next page)*

**Fig. 1.** (a) Map showing major tectonic units of the western CAOB (after Windley et al., 2007; Li et al., 2018). The inset map shows the tectonic position of the CAOB (modified after Jahn, 2004). Abbreviations: SE, Selety arc; DA, Dulate arc; YA, Yemaquan arc; BY, Balkhash-Yili arc; ZS, Zharma-Saur arc; BC, Boshchekul-Chingiz arc; BA, Baydaulet-Akbastau arc; RA, Rudny Altai; IZC, Irtysh-Zaisan Complex; AJ, Aktau-Junggar block; IMT, Ishim-Middle Tianshan block; CCT, Chinese Central Tianshan block; EY, Erementau-Yili belt; STB, South Tianshan belt; CNT, Chinese North Tianshan belt; KNTB, Kokchetav-North Tianshan belt; DVB, Early to Middle Devonian volcanic belt; NEF, North-East Fault; ISZ, Irtysh Shear Zone; CSZ, Char Shear Zone; CKF, Central Kazakhstan Fault; MTSZ, Main Tianshan Shear Zone; NNT, Nikolaiev-Nalati Fault; TFF, Talas-Fergana Fault; DF, Dalabute Fault; CANTF: Chingiz-Alakol-North Tian Shan Fault. (b) Geological map of the Chinese Altai Orogen (based on regional 1:200,000 geological maps). Granitoid ages are based on Wang et al. (2006), Zhang et al. (2012), and Tong et al. (2014b and references therein). Ages of mafic plutons are from Han et al. (2004); Wan et al. (2013), and Yang et al. (2015); High-temperature metamorphic ages are from Wang et al. (2009b, 2014b), Jiang et al. (2010), Tong et al. (2013, 2014a), Li et al. (2014), Li et al. (2015, 2017), Yang et al. (2015), Broussolle et al. (2018), Chen et al. (2019), and Liu et al. (2020b, 2020b).

Terrane (northern segment of the Kazakhstan orogenic system) by the Meso-Cenozoic Junggar Basin, comprises two late Paleozoic arcs: the Dulate Arc (in the north) and the Yemaquan Arc (in the south) (Fig. 1a). These arcs were supposedly developed in an intra-oceanic environment (Xiao et al., 2004, 2009; Zhang et al., 2009). The Dulate Arc comprises Devonian to Early Carboniferous basic/intermediate volcanic rocks and sedimentary rocks, intruded by Devonian to Permian granitoids (Zhang et al., 2006; Xiao et al., 2008; Tang et al., 2017). This arc system is separated from the Yemaquan Arc by the Armantai ophiolite belt. The latter contains Silurian marine sedimentary sequence and interlayered felsic volcanic rocks (Xu et al., 2013; Li et al., 2020a), which are overlain by Middle Devonian to Carboniferous volcanic and siliciclastic rocks (Li et al., 2020a).

## 3. Structural geology

Structural observations from the Qinghe area reveal that a number of NW–SE fold domains are separated from each other by strike-slip mylonite zones (Fig. 2a). In the Qinghe area, the Chinese Altai Orogen and the East Junggar Terrane are separated by the Mayin'erbo Fault (Qu and Zhang, 1991, 1994), which is a sinistral ductile structure here referred to as Mylonite Zone 1 (Figs. 1b and 2a). The Chinese Altai Orogen in the study area is dominated by rocks of the Ordovician Habahe Group and the Devonian Mayin'erbo Formation. The former consists mainly of metasandstone, orthogneiss, paragneiss, and mica schist (Windley et al., 2002), whereas the latter consists of meta-sandstone, meta-volcanic rocks, mica schist and minor carbonate interlayers (BGMRX, 1972). The East Junggar Terrane in the study area consists of Devonian to Carboniferous meta-volcanic/sedimentary rocks (Beitashan, Aermantie, and Nanmingshui formations) that belong to the Dulate Arc (Fig. 2a; BGMRX, 1972). The metamorphic grade recorded in these rocks (prehnite-pumpellyite facies) is distinctly lower than the metamorphic grade in the Chinese Altai Orogen, which reached amphibolite-facies conditions (BGMRX, 1972; He et al., 1990; Qu and Zhang, 1991).

### 3.1. Shear fabrics

Four NW–SE mylonite zones were mapped across the Irtysh Shear Zone (Fig. 2a). Mylonite Zone 1 (Mayin'erbo Fault) is 2.1–2.7 km wide and is characterized by a steeply dipping mylonitic foliation associated with a sub-horizontal stretching lineation (Fig. 3a, e, and 4a). Sigma-type porphyroclasts, shear band-type fragmented porphyroclasts, and S–C fabric indicate sinistral movement along Mylonite Zone 1 (Fig. 4b–d). Farther south, Mylonite zones 2–4 are narrower (<500 m). They are characterized by steeply dipping mylonitic foliation (Figs. 2 and 3b–d) and sub-horizontal stretching lineation (Fig. 3f–h). A sinistral movement is inferred from shear sense indicators, such as mica fish and sigma-type porphyroclasts (Fig. 4e–g). The structural map (Fig. 2a) shows that the extension of Mylonite zones 2 and 3 farther northwest and southeast along the strike merges into Mylonite Zone 1. Sinistral shear fabric is found along the margins of a rhomb-shaped granitic body that separates Mylonite zones 1 and 2, indicating that the granitoid was emplaced before or during deformation.

Lattice preferred orientation (LPO) in quartz was used to estimate the deformation temperature during sinistral shearing. Thin sections from ten samples were cut perpendicular to the foliation and parallel to the stretching lineation, and analyzed using electron backscatter diffraction (EBSD) in the Rock Fabric Laboratory of China University of Geosciences (Beijing) to determine quartz c-axis orientations. Quartz c-axis fabric was measured in random locations. Four samples from Mylonite Zone 1 are characterized by a dominant prism <a> slip system (Fig. 5a–d), indicating deformation temperature of 500–650 °C (Stipp et al., 2002; Passchier and Trouw, 2005; Langille et al., 2010). A mixed basal <a> slip is observed in sample L17CA132 (Fig. 5b). Five samples from Mylonite Zone 3 show variable LPO in quartz. Three samples show a dominant prism <a> slip system (Fig. 5e–g), and one sample records a rhomb <a> slip system (Fig. 5h). A mixed prism <a>, rhomb <a>, and basal <a> slip system is recorded in sample L16CA69-1 (Fig. 5i). These variable LPO patterns likely correspond to different deformation temperatures that might resulted from multiple stages of sinistral shearing along Mylonite Zone 3. Based on the occurrence of prism <a> slip, a peak deformation temperature of 500–650 °C is inferred (Stipp et al., 2002; Passchier and Trouw, 2005; Langille et al., 2010).

Along Mylonite Zone 3, dextral shear kinematics was also locally observed (in the location of sample H18CA66-2; Figs. 2a and 4h). Quartz c-axis fabrics from sample H18CA66-2 show a dominant prism <a> slip system (Fig. 5j), suggesting that dextral shearing was accompanied by relatively high temperatures (Stipp et al., 2002; Passchier and Trouw, 2005; Langille et al., 2010). Overprinting relationships between dextral and sinistral shear deformation were not observed.

### 3.2. Folds

Rocks in the areas bounded by the mylonite zones are folded and foliated. Importantly, a distinct change in the structural style is recognized across Mylonite Zone 1, which is the main boundary between the Chinese Altai Orogen and the East Junggar Terrane. The nomenclature $D_{CA1\text{-}3}$ and $D_{EJ1}$ below refers to episodes of folding in the Chinese Altai Orogen and the East Junggar Terrane, respectively.

#### 3.2.1. Chinese Altai Orogen

Rocks of the Habahe Group in the southern Chinese Altai Orogen of the study area show penetrative foliation ($S_{CA2}$; Fig. 2a), which is associated with stretching lineation ($L_{CA2}$; Fig. 6a) plunging shallowly to the southeast (Fig. 3j). An earlier fabric ($S_{CA1}$) is recognized locally in low strain zones of $D_{CA2}$, where the axial plane of rootless $D_{CA2}$ folds is parallel to $S_{CA2}$ foliation (Fig. 6b and c). In both outcrop and map scales, the $S_{CA2}$ fabric is overprinted by $D_{CA3}$ folds, which show steeply dipping axial planes trending NW–SE (Figs. 2 and 6c, d). The variable orientations of $S_{CA2}$ foliation in the map scale define a girdle, corresponding to a β axis of 32–110 (Fig. 3i). This fold axis orientation ($B_{CA32}$) is approximately parallel to the $L_{CA2}$ stretching lineation (Fig. 3j). $D_{CA3}$ folds are not associated with an axial plane fabric, indicating a low to moderate shortening strain during $D_{CA3}$ folding.

#### 3.2.2. East Junggar Terrane

Bedding ($S_{EJ0}$) can be recognized in rocks of the northern East Junggar Terrane (Nanmingshui and Beitashan formations). It is commonly steeply dipping and is folded by isoclinal to close $D_{EJ1}$ folds

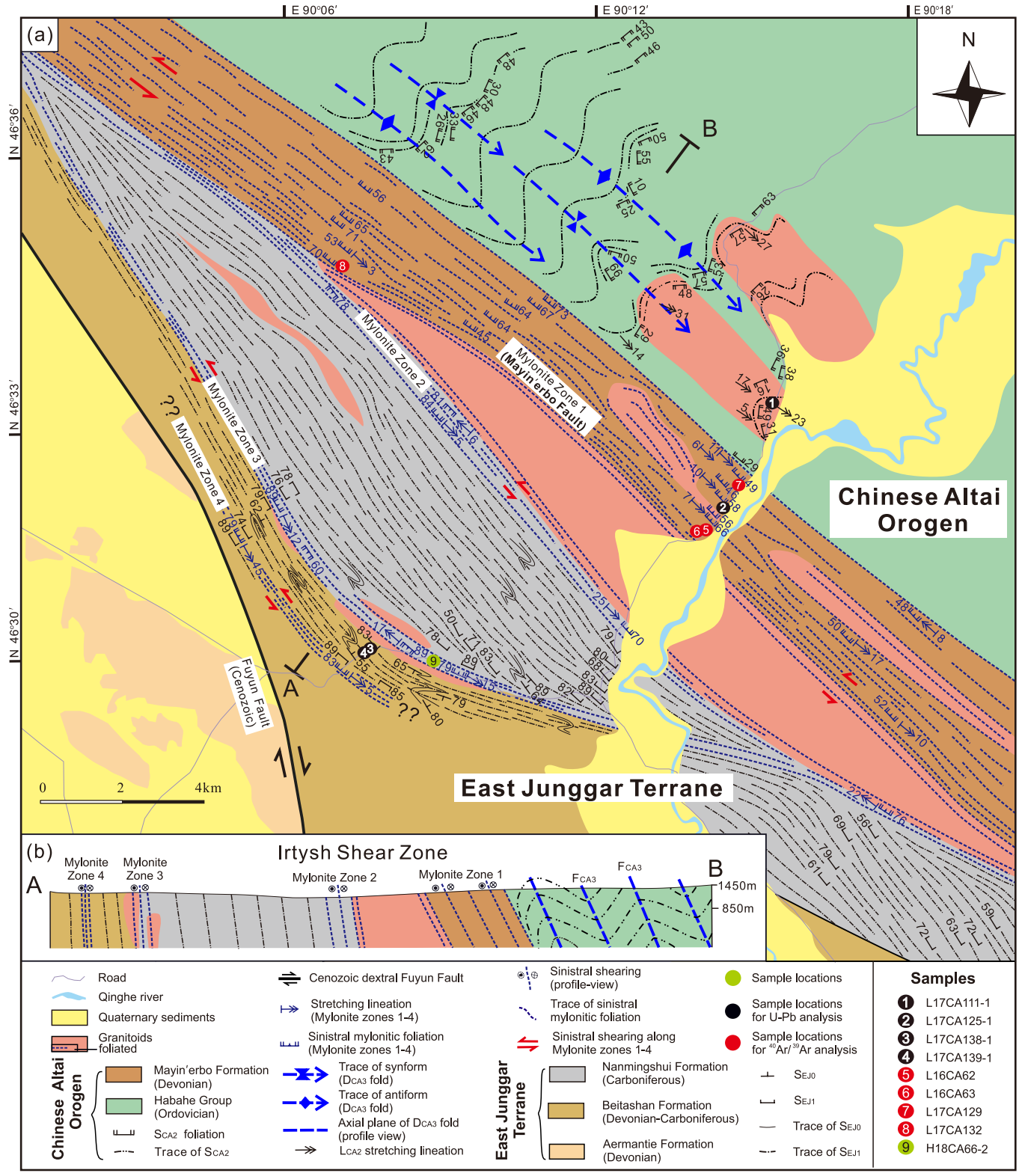


**Fig. 2.** (a) Structural map of Qinghe area, showing field observations and macroscopic structural trends (partly based on the interpretation of satellite images; Appendix A). The stratigraphic division is based on the 1:200,000 geological map (BGMRX, 1972). (b) Cross section across the Irtysh Shear Zone in the Qinghe area.

(Fig. 6e). These folds are associated with a steeply dipping NW-trending axial planar fabric ($S_{EJ1}$; Fig. 6f) that is commonly parallel or sub-parallel to $S_{EJ0}$ (Fig. 3k and l). In the southern part of the study area, $S_{EJ1}$ is truncated by Mylonite Zone 3 (Fig. 2a).

## 4. U–Pb geochronology

### 4.1. Sample description

Five samples were collected for U–Pb zircon geochronology (Figs. 1b and 2a). Sample L17CA111-1 is a gneissic granitoid from the southern

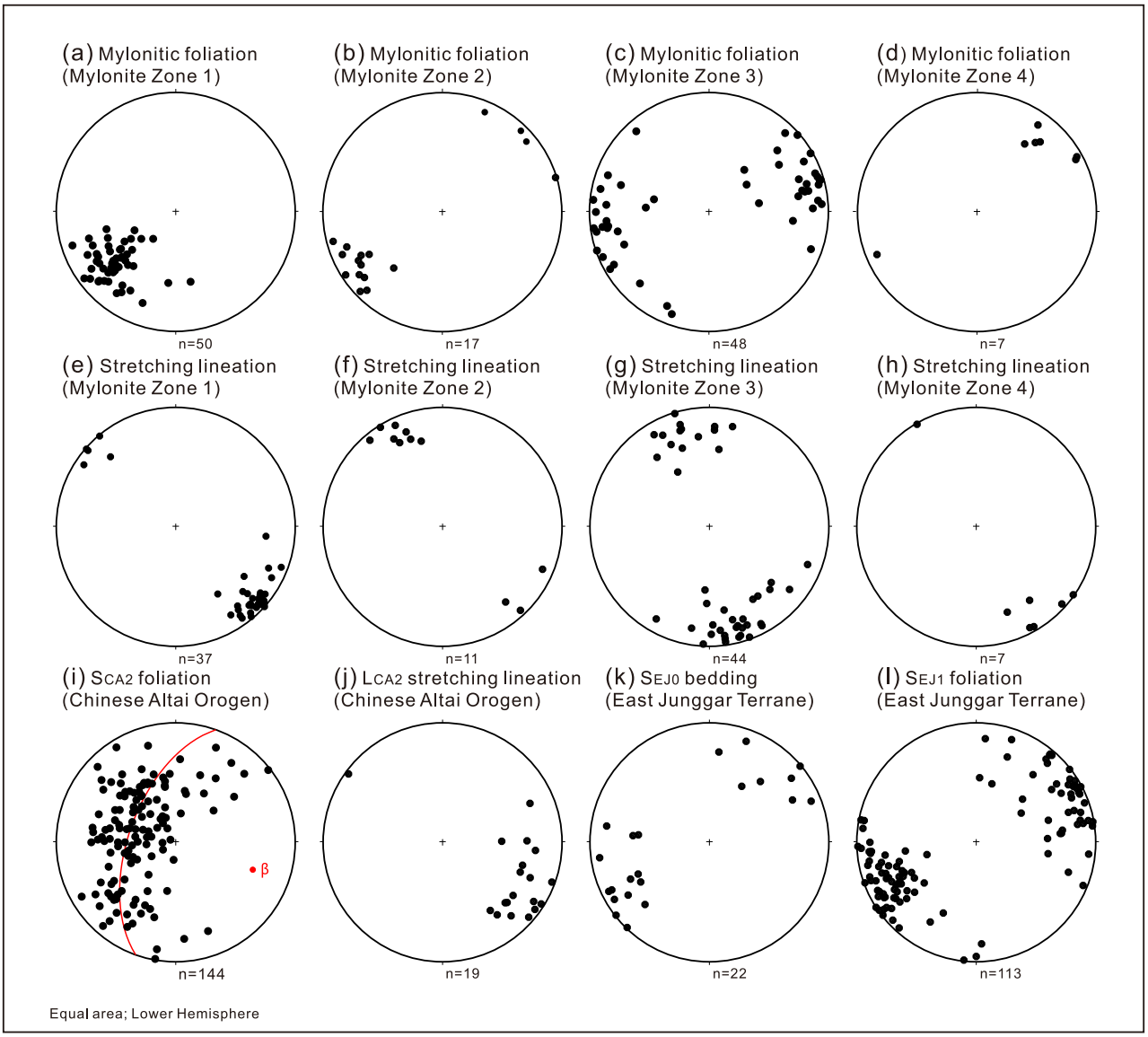


**Fig. 3.** Stereographic projection (lower hemisphere, equal area) of (a–h) mylonitic foliation and stretching lineation in Mylonite zones 1–4, and (i–l) structural fabric and bedding in the folded zones.

Chinese Altai Orogen (Fig. 2a), composed mainly of quartz, plagioclase and minor biotite. The sample shows a penetrative $S_{CA2}$ foliation (Fig. 7a). Therefore, its zircon crystallization age can constrain the maximum age of $D_{CA2}$.

Four samples were targeted for detrital zircon analysis. Sample L17CA125-1 is from the Mayin'erbo Formation (southern Chinese Altai Orogen; Fig. 2a). It is a dark gray mica schist with a mylonitic fabric (Fig. 7b). Two poorly sorted sandstone samples (L17CA138–1 and L17CA139-1; Fig. 7c and d) are from the Beitashan Formation (Dulate Arc, East Junggar Terrane; Fig. 2a). Sample L17CA138-1 is composed mainly of fine-grained quartz, feldspar, and minor opaque minerals, and sample L17CA139-1 is dominated by quartz, plagioclase, opaque minerals, and minor muscovite. Sample H18CA75-1 is from the Nanmingshui Formation (southern Dulate Arc, East Junggar Terrane; Fig. 1b). It is a fine-grained sandstone that contains sub-angular quartz, feldspar, sedimentary/volcanic lithic fragments, and minor opaque minerals (Fig. 7e).

### 4.2. Methods

Zircon grains were obtained by conventional heavy fraction and magnetic techniques. The grains were then mounted in an epoxy resin. Inclusions and fractures were observed and imaged using a transmitted and reflected light microscope, and cathodoluminescence (CL) images were taken by a field emission-scanning electron microprobe (JXA8100, JEOL) equipped with a Gatan Mono CL3 system at the Guangzhou Institute of Geochemistry, Chinese Academy of Sciences (GIG-CAS). All mounts were polished to expose zircon surfaces suitable for analysis. Zircon U–Pb dating was conducted with a laser ablation inductively coupled plasma mass spectrometry (LA-ICP-MS) (Resonetics RESOlution S-155 laser ablation system combined with an Agilent 7900) at GIG-CAS. The laser spot size of in-situ measured analysis was 29 μm. To reduce the statistical error caused by laser ablation pulse and improve the data quality, a squid smoothing device was designed (Liu et al., 2010). The Pb/U ratio was calibrated relative to the standard zircon 91500 and the Plešovice standard (Sláma et al., 2008; Liu et al., 2010). Detailed analytical procedures are documented in Liu et al. (2010). ICPMSDataCal 10.8 software was used for U–Pb data reduction, and the ISOPLOT program was used to calculate the weighted mean age and to produce concordia and age probability plots (Ludwig, 2003).

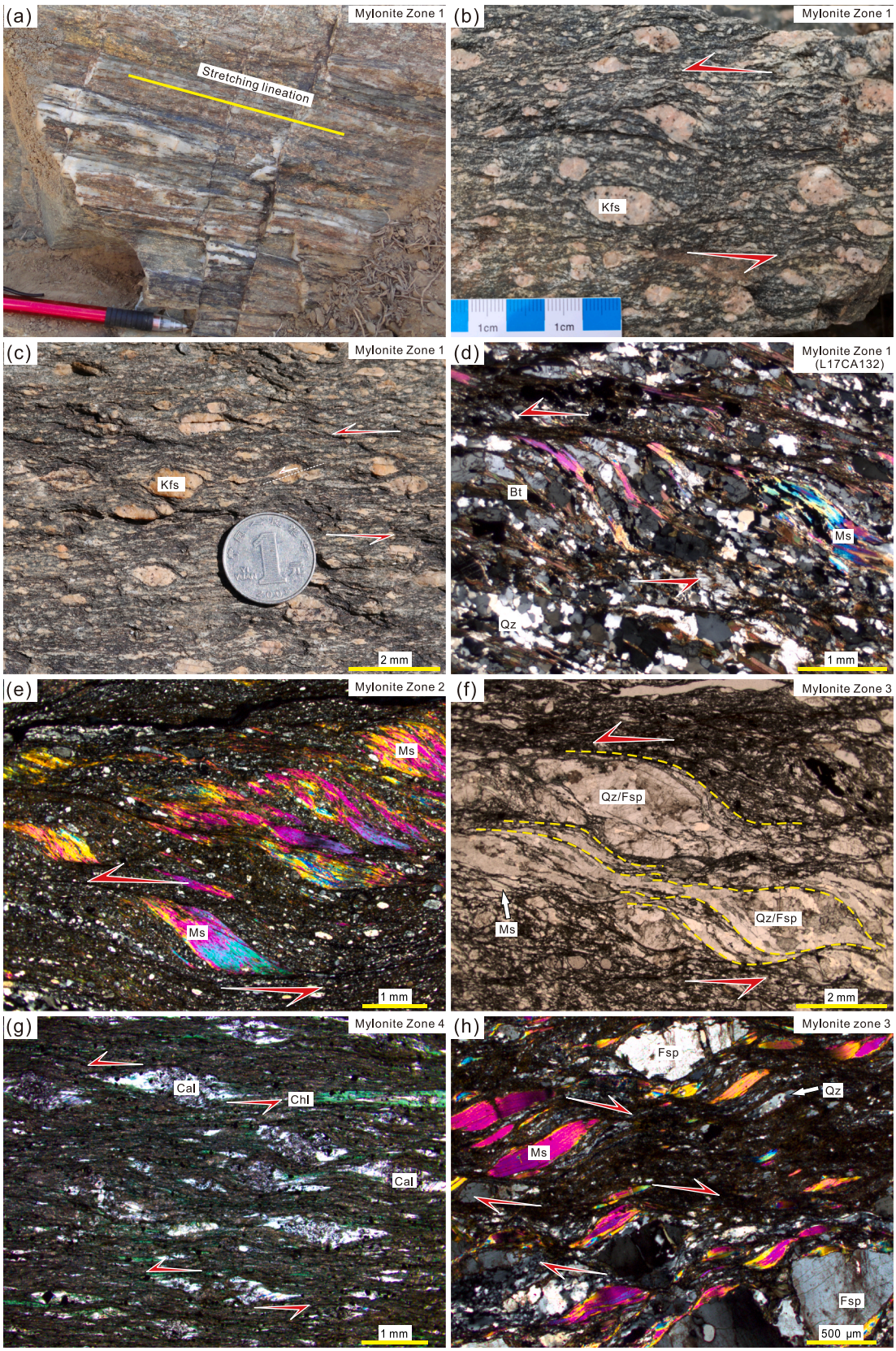


**Fig. 4.** Photographs from Mylonite zones 1–4. (a) Stretching lineation defined by stretched quartz aggregates (Mylonite Zone 1). (b–d) Sinistral shearing indicated by sigma-type porphyroclasts, shear bands between fragmented porphyroclasts, and S–C fabric (Mylonite Zone 1). (e–g) Sinistral shearing indicated by mica fish and sigma-type porphyroclasts (Mylonite zones 2–4). (h) Evidence of local dextral shearing indicated by mica fish (Mylonite Zone 3; see the location of sample L18CA66-2 in Fig. 2a). Abbreviation: Kfs, K-feldspar; Bt, biotite; Ms, muscovite; Qz, quartz; Qz/Fsp: quartz-feldspar aggregate; Cal, calcite; Chl, chlorite; Fsp, feldspar.

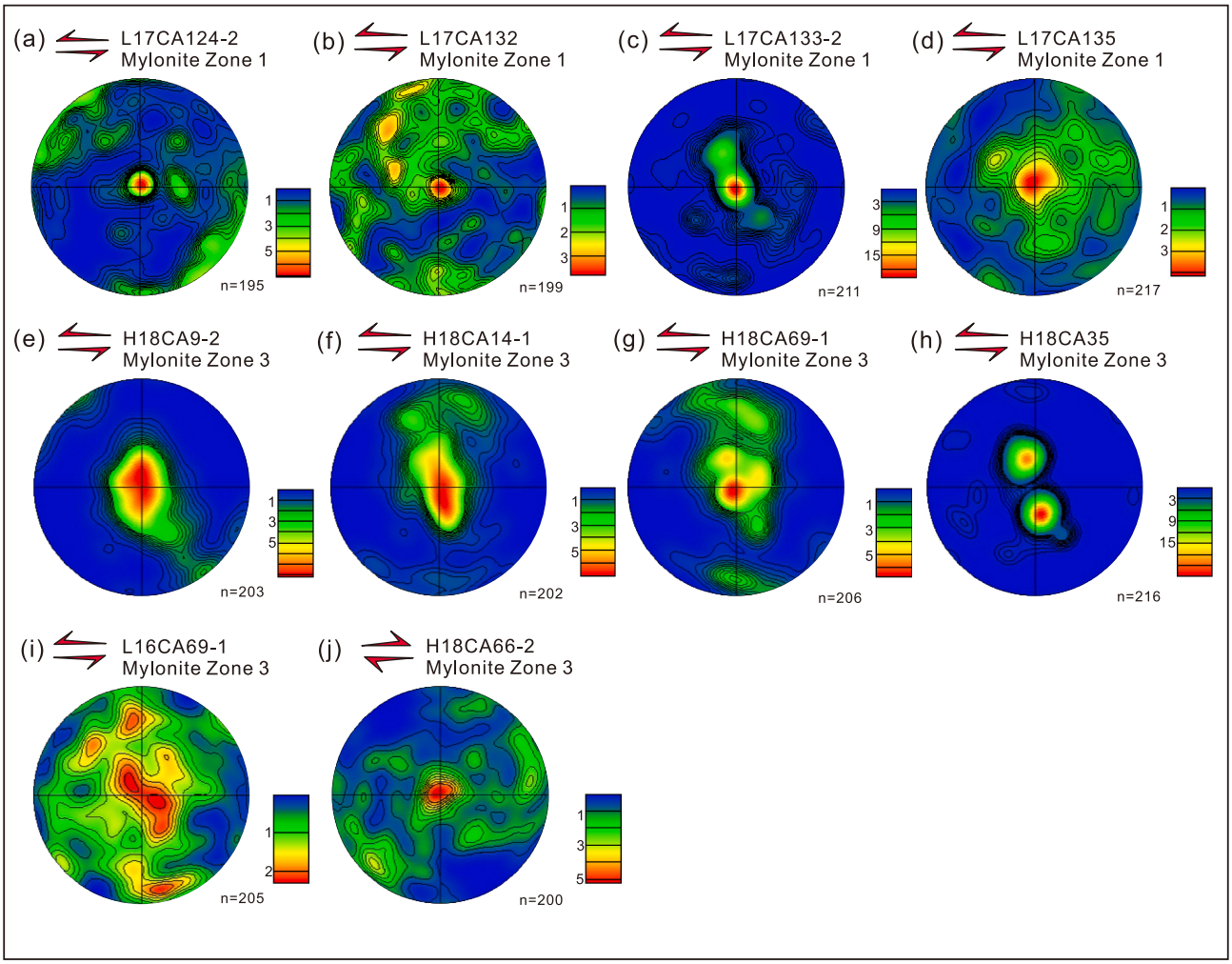


**Fig. 5.** Quartz c-axis fabrics in mylonitic rocks from Mylonite zones 1 and 3 (lower hemisphere, equal area projection; n = number of data points). The contours at multiples of a mean uniform density with higher values indicated by red color. (For interpretation of the references to color in this figure legend, the reader is referred to the Web version of this article.)

### 4.3. Results

CL images and ages of the representative zircon grains are presented in Fig. 8, and the U–Pb data are presented in Appendix B. Zircon ages (<10% discordance) are plotted in probability density and concordia diagrams (Fig. 9). $^{206}Pb/^{238}U$ ages are used for zircon grains younger than 1000 Ma, whereas $^{207}Pb/^{206}Pb$ ages are used for zircon grains older than 1000 Ma.

Zircon grains from the foliated granitoid (sample L17CA111-1) are elongated with length/width ratios of 1:2–1:4. Most of the grains are characterized by brightly luminescent oscillatory zones (Fig. 8a) and Th/U ratios of 0.17–0.95, thus indicating an igneous origin. Two anomalously old concordant ages of ~325 Ma and ~443 Ma (Fig. 9a), which might represent inherited components, were excluded for the calculation of the weighted mean age. After excluding another four discordant ages, the rest of 27 analyses yielded a weighted mean $^{206}Pb/^{238}U$ age of 288.1 ± 3.6 Ma (MSWD = 1.2; Fig. 9a and b).

Detrital zircon grains from sample L17CA125-1 (Chinese Altai Orogen) are generally rounded, but some idiomorphic prisms were also found. The grains show oscillatory zoning. Grain sizes are 50–200 μm. Core-rim structures were not observed. The CL images show low to high luminescence (Fig. 8b). The Th/U ratios of 0.2–1.3 suggest an igneous origin. Out of 64 analyses, four zircon grains yielded anomalously young (<360 Ma) scattered ages, which are younger than the age of deposition. These ages might have resulted from Pb loss. After excluding these outliers, a broad range of detrital zircon ages was obtained, with prominent peaks at ~469 Ma, ~499 Ma, and ~518 Ma, and minor peaks at ~388 Ma, ~622 Ma, ~743 Ma, and ~937 Ma (Fig. 9c and d). A few zircon grains from this sample yielded Paleoproterozoic and Mesoproterozoic ages (Fig. 9c and d).

Detrital zircon grains from samples L17CA138–1, L17CA139-1, and H18CA75-1 (Dulate Arc, East Junggar Terrane) are euhedral (60–240 μm). CL images of these zircon grains show mostly oscillatory or sector zoning (Fig. 8c–e), which together with the evidence of moderate Th/U ratios (0.3–1.3), indicate an igneous origin. Grains from sample L17CA138-1 yielded 55 U–Pb ages ranging from 320 Ma to 380 Ma, with a prominent peak at ~351 Ma (Fig. 9e and f). A similar zircon population is found in sample L17CA139-1 (56 analyses), with a major peak at ~349 Ma and a minor peak at ~371 Ma (Fig. 9g and h). Detrital zircon grains from sample H18CA75-1 (56 analyses) yielded ages of 375–315 Ma with clusters at ~332 Ma and ~371 Ma (Fig. 9i and j).

## 5. $^{40}Ar/^{39}Ar$ geochronology

### 5.1. Sample description

$^{40}Ar/^{39}Ar$ dating was used to constrain the timing of sinistral shearing. We collected four samples along Mylonite Zone 1 (Fig. 2a). These samples are characterized by a pervasive mylonitic fabric with sinistral shear sense criteria (Figs. 4d and 7f). Samples L16CA62 and

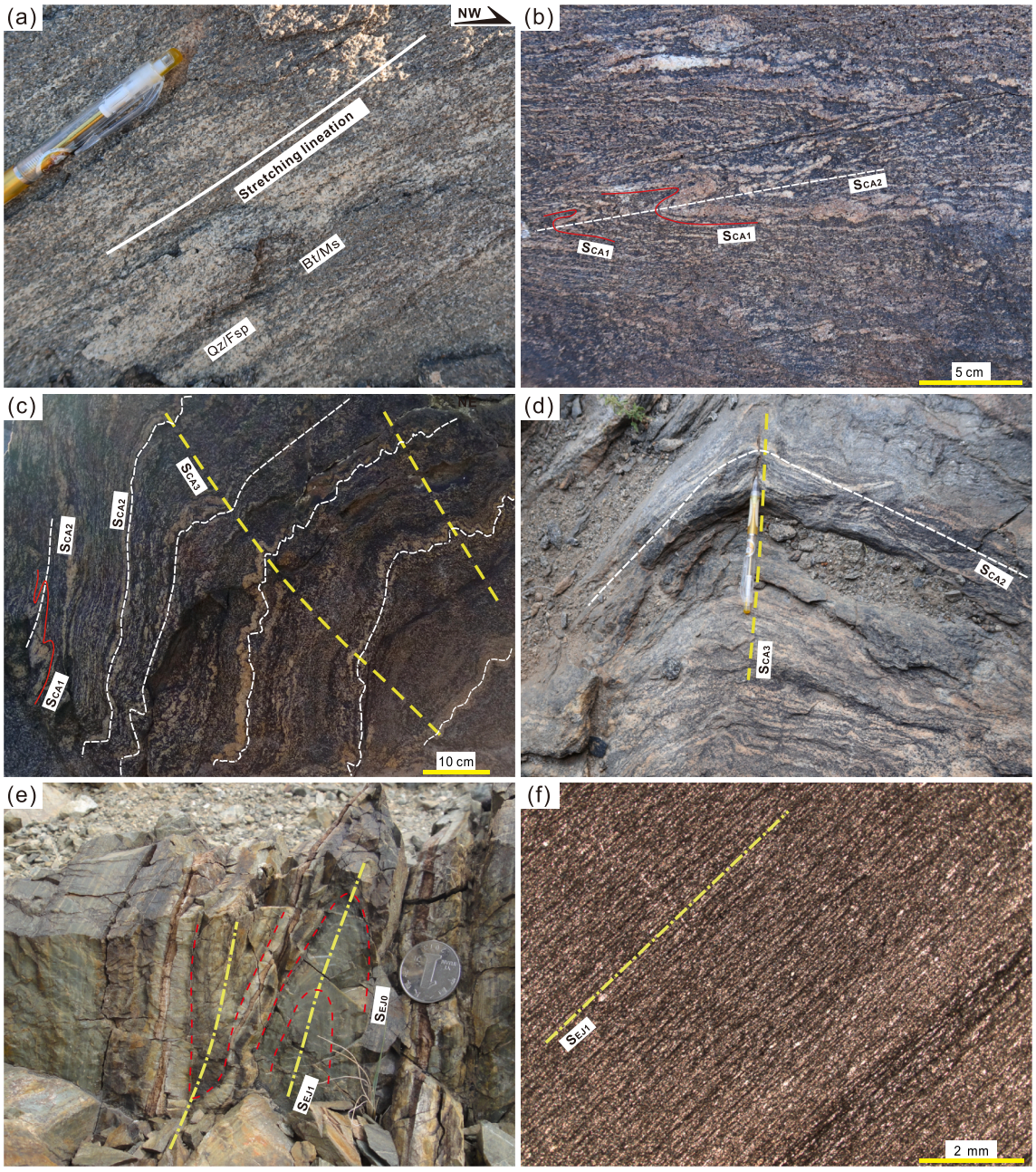


**Fig. 6.** Photographs from folded zones in the southern Chinese Altai Orogen (a–d) and the northern East Junggar Terrane (e–f). (a) Shallowly southeast-plunging stretching lineation ($L_{CA2}$) defined by quartz and feldspar aggregates. (b) Folded $S_{CA1}$ foliation in a low strain area of $D_{CA2}$. $S_{CA1}$ is transposed by the dominant $S_{CA2}$ fabric. (c–d) $S_{CA2}$ foliation folded by $D_{CA3}$ folds. Note the rootless $D_{CA2}$ fold in (c), which shows transposed $S_{CA1}$ foliation. (e) Tightly folded bedding ($S_{EJ0}$) forming $D_{EJ1}$ folds. (f) $S_{EJ1}$ axial planar fabric with microlithons and cleavage domains defined by quartz and clay-rich material, respectively.

L16CA63 were taken from two localities ~40 m from each other (Figs. 2a and 7f, g). Both samples are granitic mylonite, consisting of quartz, feldspar, biotite, and muscovite (Fig. 7f and g). Samples L17CA129 and L17CA132 are mica schist, composed mainly of quartz, feldspar, biotite and muscovite (Figs. 4d and 7h).

### 5.2. Methods

Samples were crushed and then cleaned in distilled water and absolute ethanol with an ultrasonic wash. Unaltered pure biotite and muscovite were selected using a binocular. Both biotite and muscovite were selected from samples L16CA62 and L16CA63. From samples L17CA129 and L17CA132, muscovite was separated. Mineral grains were loaded into an aluminum disc with five large wells (0.3 cm depth and 1.9 cm diameter), together with the Fish Canyon sanidine standard (28.294 Ma; Renne et al., 2011). Samples were then irradiated for 30 h in the TRIGA nuclear reactor in Oregon State University (USA) in a central position. Samples were analyzed at the Western Australian Argon Isotope Facility at Curtin University. A detailed description of the analytical procedure can be found in Li et al. (2020b). The ArArCALC-software (Koppers, 2002) was used for data processing. For the age calculation, we used the decay constants recommended by Renne et al. (2011). Plateau ages were defined when at least three consecutive steps contained >70% $^{39}$Ar. The fitting probability (P) is at least 0.05. Uncertainties of the plateau ages are given at the 2σ level. Mini-plateau ages, defined as containing between 50% and 70% of the $^{39}$Ar released, are deemed as less robust than the plateau ages.

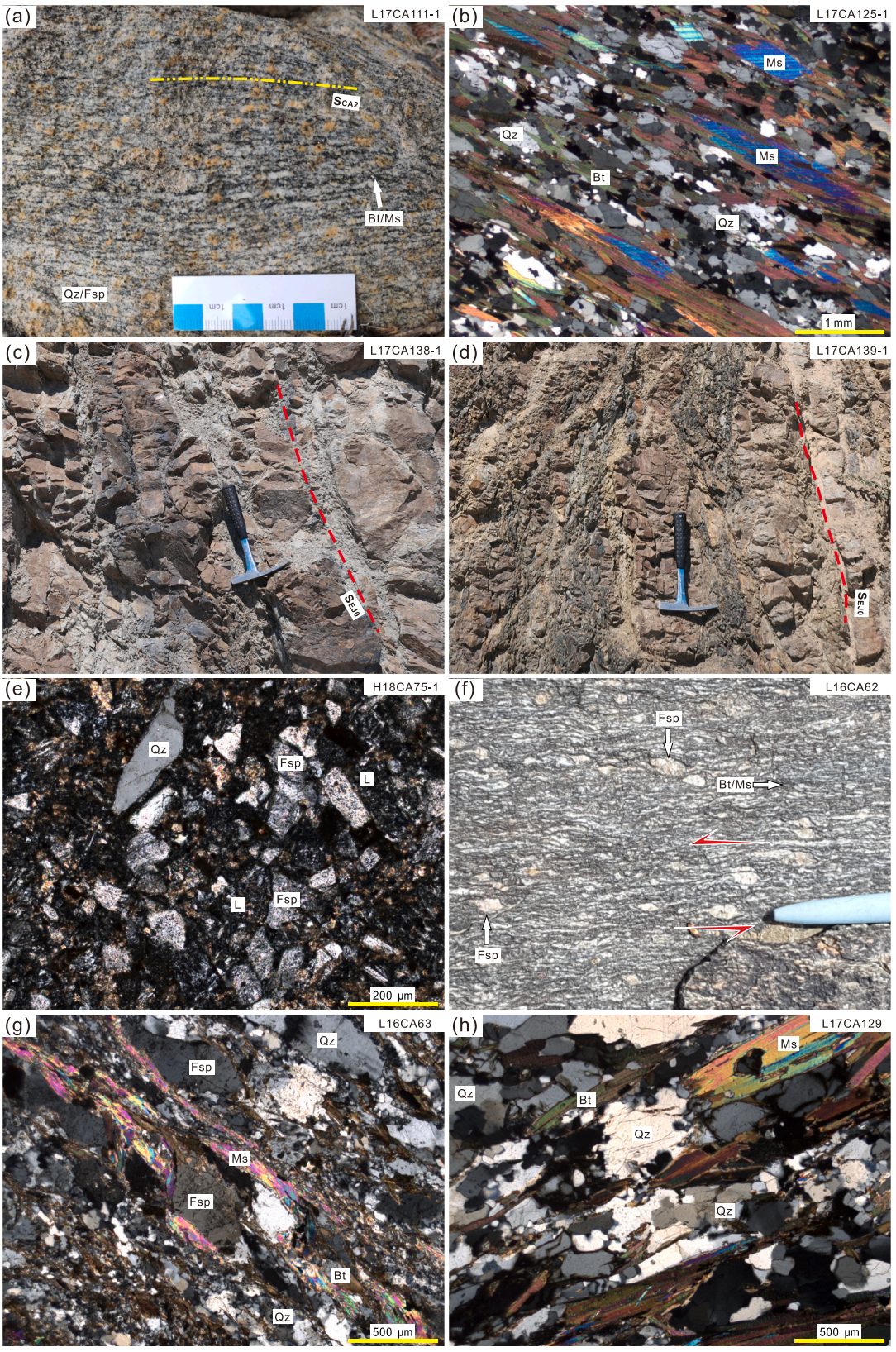


**Fig. 7.** Photographs of the samples used for zircon U–Pb dating (a–e) and $^{40}Ar/^{39}Ar$ dating (f–h). (a) Gneissic granitoid with penetrative $S_{CA2}$ foliation. (b) Mica schist with preferred alignment of muscovite and biotite to define a mylonitic fabric. (c–d) Interlayered sandstones from the Beitashan Formation of the Dulate Arc. (e) Sandstone from the Nanmingshui Formation of the southern Dulate Arc, containing mainly sub-angular quartz, feldspar, sedimentary/volcanic lithic fragments. (f) Granitic mylonite with preferred alignment of muscovite and biotite to define a mylonitic fabric. Sinistral shearing is indicated by sigma-type feldspar porphyroclasts. (g) Preferred alignment of muscovite and biotite to define a mylonitic fabric in granitic mylonite. Note that samples L16CA62 in Fig. 7f and L16CA63 in Fig. 7g were taken from two localities ~40 m from each other (Fig. 2a). (h) Mica schist with a mylonitic fabric defined by oriented muscovite/biotite and quartz ribbon. Abbreviations: Qz, quartz; Fsp, feldspar; Ms, muscovite; Bt, biotite; L, lithic fragments.

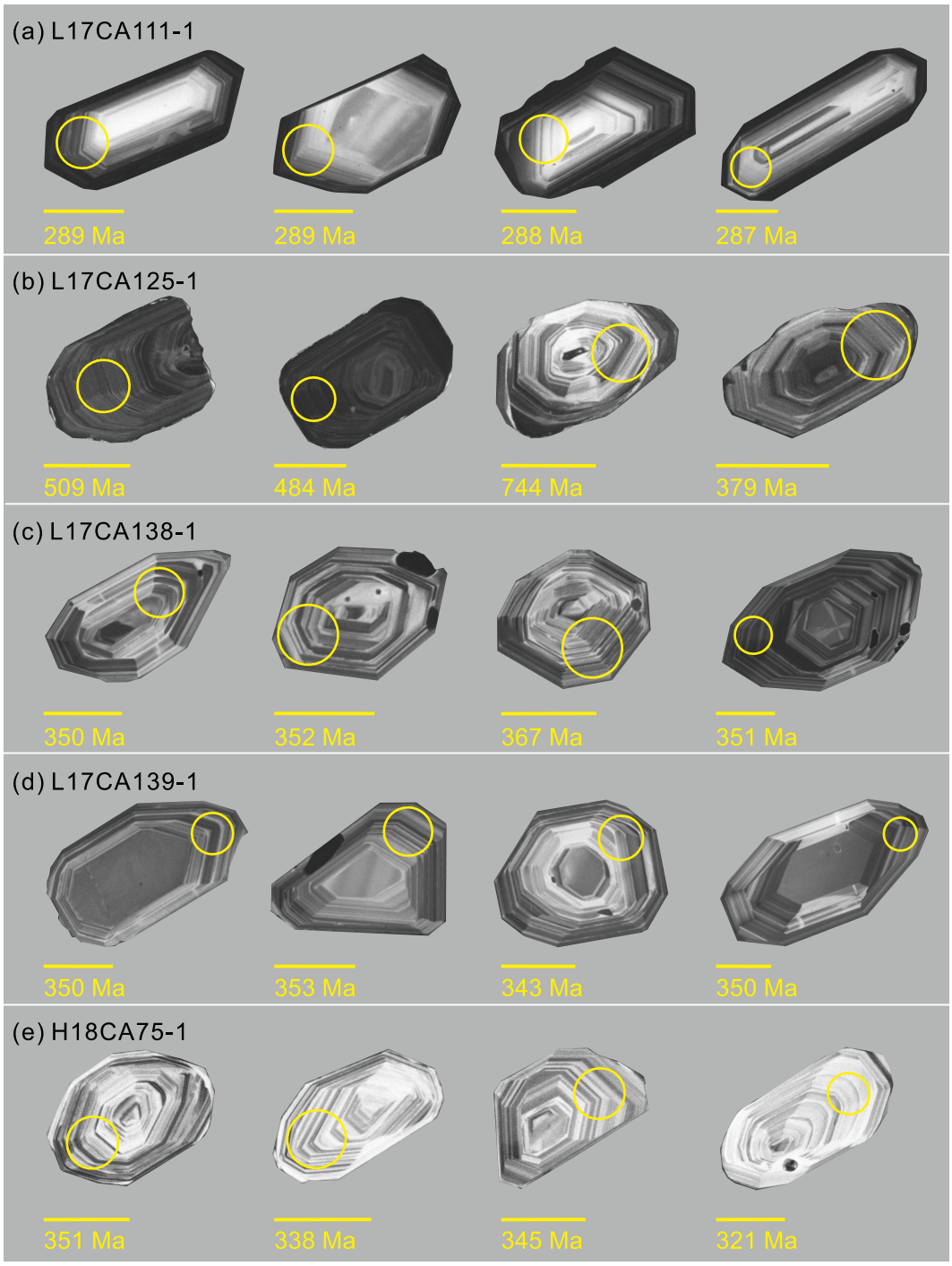


**Fig. 8.** Representative CL images of zircon grains and corresponding $^{206}Pb/^{238}U$ ages. Locations of dated spots are indicated by circles. The length of the yellow scale bar is 50 μm. (For interpretation of the references to color in this figure legend, the reader is referred to the Web version of this article.)

### 5.3. Results

$^{40}Ar/^{39}Ar$ results are presented in Fig. 10 and Appendix C. All biotite and muscovite grains show relatively flat age spectra. Two biotite grains from samples L16CA62 and L16CA63 yielded two plateau/mini-plateau ages of 265.1 ± 1.8 Ma (Fig. 10a; MSWD = 1.1; P = 0.36) and 270.4 ± 1.5 Ma (Fig. 10c; MSWD = 0.5; P = 0.76), respectively. Three muscovite grains from samples L16CA63, L17CA129 and L17CA132 yielded plateau ages of 268.0 ± 1.1 Ma (Fig. 10d; MSWD = 1.0; P = 0.44), 273.3 ± 0.4 Ma (Fig. 10e; MSWD = 0.6; P = 0.83), and 269.1 ± 0.3 Ma (Fig. 10f; MSWD = 1.9; P = 0.07), respectively. Another muscovite grain from sample L16CA62 did not yield a plateau age (Fig. 10b), but provided steps with a similar range.

## 6. Discussion

### 6.1. Timing of deformation

#### 6.1.1. Timing of strike-slip deformation

Our structural observations show that Mylonite zones 1–4 were subjected predominantly to sinistral deformation. Two syn-kinematic biotite from Mylonite Zone 1 gave $^{40}Ar/^{39}Ar$ ages of 270–265 Ma,

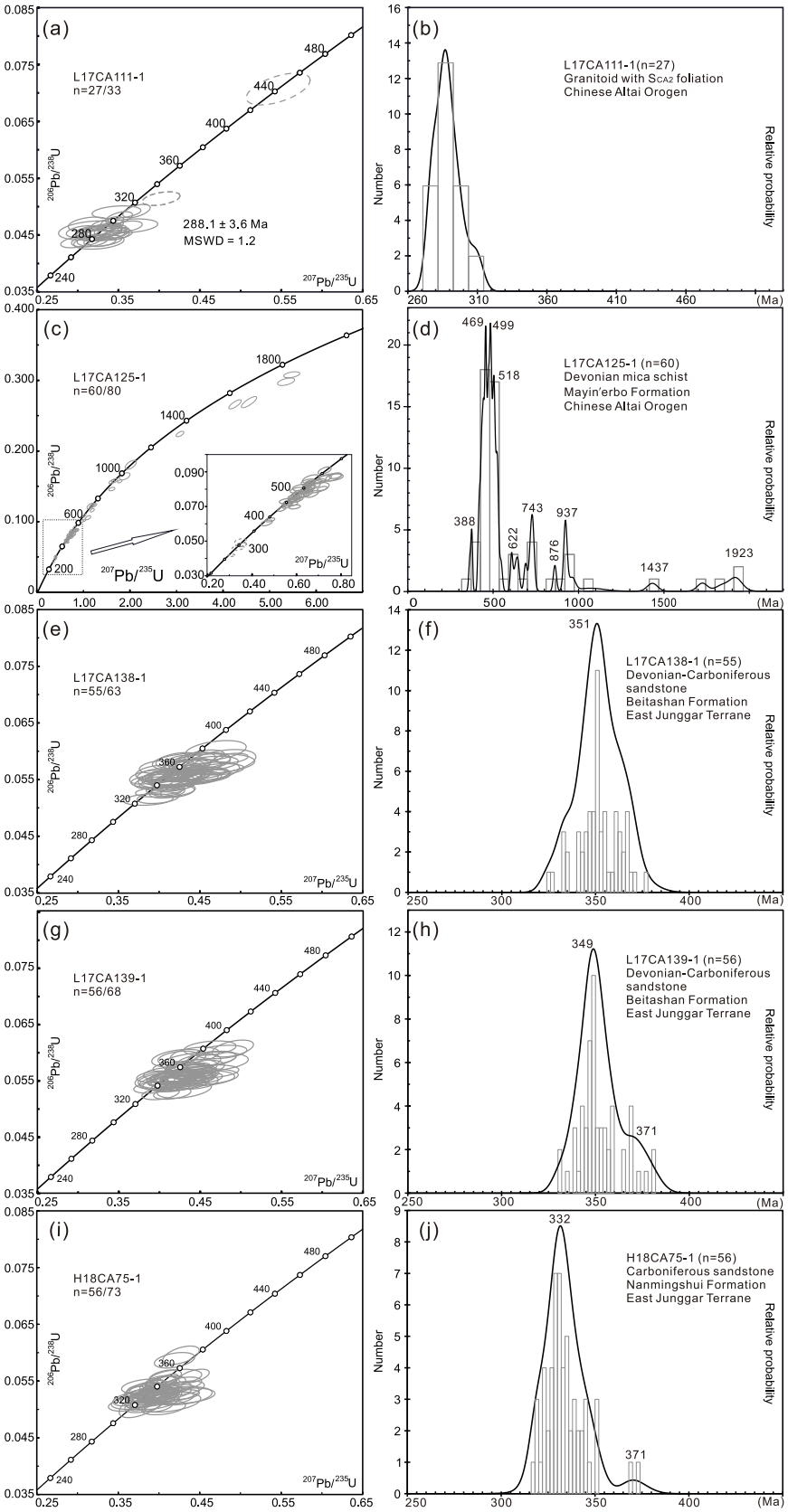


**Fig. 9.** U–Pb concordia diagrams (left) and age probability diagrams (right) of analyzed zircon grains. Ellipses represent errors at 1σ level. The dotted ellipses in Fig. 9a are excluded from the age calculation. Note that four ages younger than deposition ages in sampleL17CA125-1 (Fig. 9c) are not plotted in the age probability diagram (Fig. 9d).

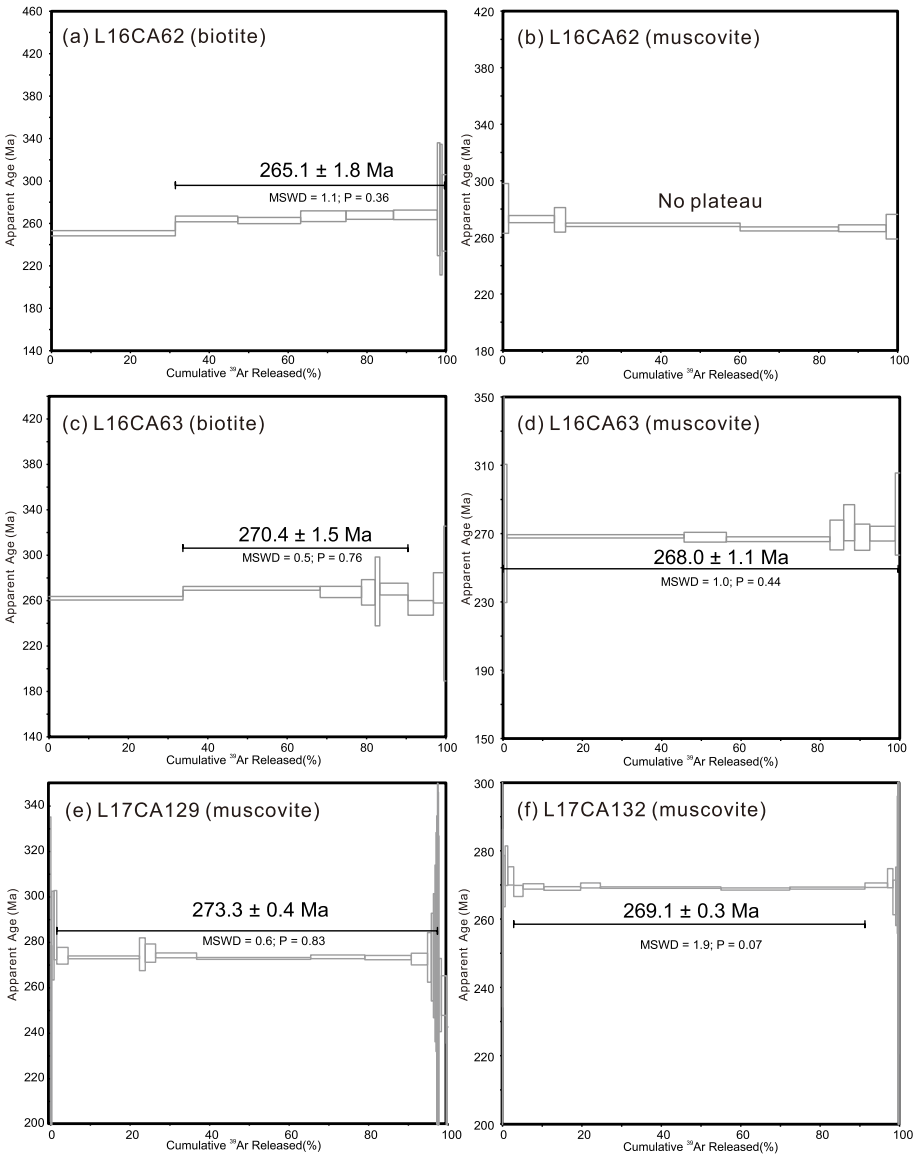


**Fig. 10.** $^{40}Ar/^{39}Ar$ step-heating age spectra showing individual steps plotted against the cumulative percentage of $^{39}Ar$ release. The error of uncertainty is given at 2σ. The MSWD and probability (P) of plateau ages are also shown.

whereas the muscovite samples from the same mylonite zone yielded $^{40}Ar/^{39}Ar$ ages ranging from 273 Ma to 268 Ma. These ages could either represent the timing of crystallization of the analyzed minerals, or the timing of cooling below the closure temperature. The quartz c-axis fabric of four samples from Mylonite Zone 1 shows a dominant prism <a> slip system (Fig. 5a–d) that indicates deformation temperatures of 500–650 °C (Stipp et al., 2002; Passchier and Trouw, 2005; Langille et al., 2010). These temperatures are higher than the closure temperatures of biotite and muscovite (365 ± 35 °C and 425 ± 70 °C, respectively; Scibiorski et al., 2015), thus suggesting that the $^{40}Ar/^{39}Ar$ ages represent the timing of cooling below the closure temperatures. One sample (L16CA63) from Mylonite Zone 1 yielded a biotite $^{40}Ar/^{39}Ar$ age of 270.4 ± 1.5 Ma (Fig. 10c), which overlaps within error with the 268.0 ± 1.1 Ma muscovite age from the same sample (Fig. 10d). This indicates a fast cooling of the analyzed sample, possibly in response to sinistral transpression (see more discussion in Section 6.2; e.g. Sanderson and Marchini, 1984; Zhang et al., 2012; Cao and Neubauer, 2016). Therefore, we think that the 273–265 Ma $^{40}Ar/^{39}Ar$ ages represent the timing of sinistral shearing.

It is possible that sinistral shearing in the southern Chinese Altai Orogen had commenced prior to 273 Ma. In the Fuyun area (Fig. 1b), syn-shearing hornblende and biotite yielded $^{40}Ar/^{39}Ar$ ages of ~283 Ma ages (Fig. 12; Li et al., 2017). These ages are interpreted to represent the timing of sinistral shearing along the Irtysh Shear Zone. Together with our new ages, it appears that the Irtysh Shear Zone was subjected to multiple stages of sinistral shearing from ~283 Ma to ~265 Ma.

In Mylonite Zone 3 (Fig. 2a), evidence of dextral shear fabric was also recognized locally (Fig. 4h). Dextral shear fabrics were reported in other areas along the Southern Chinese Altai Orogen (Laurent-Charvet et al., 2003; Liu et al., 2013), but overprinting relationships with the sinistral shear deformation has not been observed. It is therefore difficult to understand the timing and regional context of this deformation. According to Laurent-Charvet et al. (2003), dextral shearing occurred at a late stage of the tectonic evolution, following the earlier sinistral strike-slip deformation. Based on our observations, we are unable to support or refute this interpretation.

### 6.1.2. *Timing of folding*

Three generations of structures ($D_{CA1}$–$D_{CA3}$) were observed in the southern Chinese Altai Orogen, north of Mylonite Zone 1. The earliest

generation of fabric ($D_{CA1}$) is only observed locally and its age is poorly constrained. The dominant foliation ($D_{CA2}$) affected granitoid bodies (Fig. 2a), such as the one represented by sample L17CA111-1, which shows a pervasive $D_{CA2}$ fabric (Fig. 7a). This sample yielded a $^{206}Pb/^{238}U$ age of 288.1 ± 3.6 Ma (Fig. 9a and b), thus indicating that deformation occurred after 288 Ma. The timing of NW–SE folding ($D_{CA3}$) is not directly constrained. However, NW–SE folds, which widely occur within the southern Chinese Altai Orogen (Qu and Zhang, 1994; Briggs et al., 2009; Li et al., 2015, 2016a; 2016b; Jiang et al., 2019) are cut by ~ NE–SW granitic dykes (Fig. 1b; Li et al., 2015), which yielded U–Pb zircon ages as young as ~252 Ma (Zhang et al., 2012). Therefore, deformation must have occurred during the Permian, prior to the emplacement of these dykes.

A single phase of folding ($D_{EJ1}$) is recognized in the East Junggar Terrane. This deformation must have occurred after the deposition of the deformed Nanmingshui Formation (Fig. 2a). The youngest detrital zircon age peak in sample H18CA75-1, from this formation, is ~332 Ma (Fig. 9j), thus providing a maximum constraint on the timing of deformation.

### 6.2. Tectonic implications

#### 6.2.1. When did the East Junggar Terrane collide with the Chinese Altai Orogen?

The Mayin'erbo Fault (Mylonite Zone 1; Fig. 2a) has previously been described as the boundary between the Chinese Altai Orogen and the East Junggar Terrane (Mylonite Zone 1; Fig. 2a; Qu and Zhang, 1994; Laurent-Charvet et al., 2002, 2003). Our new detrital zircon data support this interpretation. Our data show that sedimentary rocks from the Dulate Arc of the northern East Junggar Terrane (samples L17CA138–1, L17CA139-1, and H18CA75-1) do not contain detrital zircon grains older than the early Paleozoic (Fig. 9e–j). In the Chinese Altai Orogen, in contrast, Proterozoic to early Paleozoic ages are widespread (Long et al., 2007; Jiang et al., 2011; Wang et al., 2014c; Li et al., 2017, 2019). Along the Mayin'erbo Fault, Devonian meta-volcanic and meta-sedimentary rocks of the Mayin'erbo Formation are strongly deformed by sinistral shear deformation (Fig. 2a). A mica schist sample from this formation (L17CA125-1) yielded a detrital zircon age population of ~469 Ma, ~499 Ma, and ~518 Ma (major peaks), and ~388 Ma, ~622 Ma, ~743 Ma, and ~937 Ma (minor peaks) (Fig. 9d). This pattern of detrital zircon ages corresponds to zircon age populations from the Chinese Altai Orogen (Fig. 11a and b), thus confirming that the Mayin'erbo Formation represents the southernmost part of the Chinese Alai Orogen (Qin et al., 1991; Qu and Zhang, 1991; Hong et al., 2015).

Previous constraints on the timing of collision between the East Junggar Terrane and the Chinese Altai Orogen have been based on the geochemistry of igneous rocks. These studies have suggested a collision during the earliest Carboniferous (Tong et al., 2012), Late Carboniferous (Tong et al., 2014b; Zhang et al., 2018), and Permian (post to ~276 Ma; Wan et al., 2013). However, these interpretations are inconclusive, because of the difficulty in determining the exact origin of magmatic rocks, which are commonly contaminated by variable crustal materials and/or derived from inherited metasomatized mantle components (e.g., Wang et al., 2014c).

Our new detrital zircon data provide an independent constraint on the timing of collision. Devonian to Carboniferous detrital zircon populations in samples from the Dulate Arc of the East Junggar Terrane (Qinghe area; Fig. 11c) are correlated to detrital zircon ages in the Fuyun area (Fig. 11d; Nie et al., 2014; Li et al., 2017, 2019). These detrital zircon grains were likely sourced from Devonian–Carboniferous magmatic rocks in the Dulate Arc (Zhang et al., 2006, 2009; Liang et al., 2016; Li et al., 2019). In the Qinghe area, Early Carboniferous detrital zircon grains are abundant in samples L17CA138-1 and L17CA139-1 from the Beitashan Formation (Dulate Arc; Fig. 9f and g), thus providing a maximum age of deposition for this formation, which was previously considered Middle Devonian in age (BGMRX, 1972).

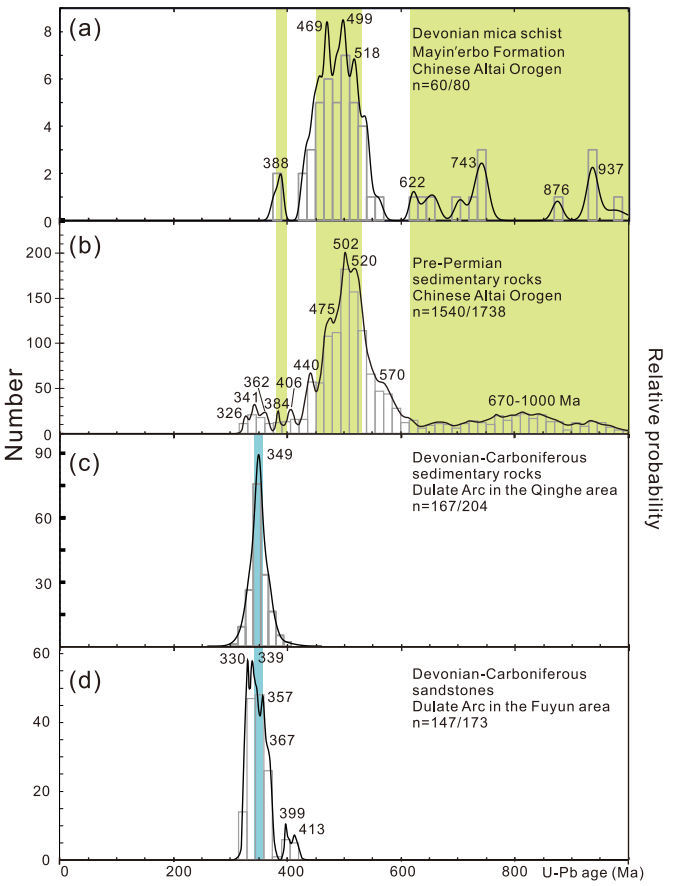


**Fig. 11.** Age probability diagrams of detrital zircon grains from this study (a, c), and a comparison with previously published detrital zircon populations from the Chinese Altai Orogen (b) and the Dulate Arc of the northern East Junggar Terrane (d) (Li et al., 2019). Detrital zircon populations from a Devonian mica schist of the Mayin'erbo Formation (Fig. 11a), are compatible with detrital zircons from the Chinese Altai Orogen (Fig. 11b). Detrital zircon ages from Devonian-Carboniferous sedimentary rocks are correlated in both Qinghe and Fuyun areas (Fig. 11c and d).

Carboniferous samples from both the Nanmingshui and Beitashan formations (Dulate Arc) do not contain detrital zircon grains that were derived from the Chinese Altai Orogen, thus indicating that during the deposition of these rocks, the Dulate Arc was likely separated from the Chinese Altai Orogen by the Ob-Zaisan Ocean. The youngest detrital zircon age peak of ~332 Ma (Fig. 9j) in the Dulate Arc provides a maximum constraint on the timing of deposition, and further indicates that the closure of the Ob-Zaisan Ocean occurred after ~332 Ma. This conclusion is consistent with constraints on the timing of ocean closure in the Fuyun area father west, where rocks from the Dulate Arc yielded a youngest age peak of ~330 Ma (Fig. 11d; Li et al., 2017). During this period, an accretionary wedge (Ohara et al., 1997; Briggs et al., 2007; Xiao et al., 2009) was developed along the southern margin of the Chinese Altai Orogen (Irtysh Complex; Fig. 1b). This accretionary complex was still active at ~322 Ma (Fig. 12), as constrained by the youngest population of detrital zircon grains (Li et al., 2015). On the other hand, the closure of the Ob-Zaisan Ocean must have occurred prior to the initiation of sinistral shearing along the Irtysh Shear Zone at ~283 Ma (Li et al., 2017), which marks the boundary between the Chinese Altai Orogen and the East Junggar Terrane. Therefore, the timing of collision is constrained to 322–283 Ma.

#### 6.2.2. Implications for collisional processes of the East Junggar Terrane and the Chinese Altai Orogen

Previous authors have suggested that the collision of the East

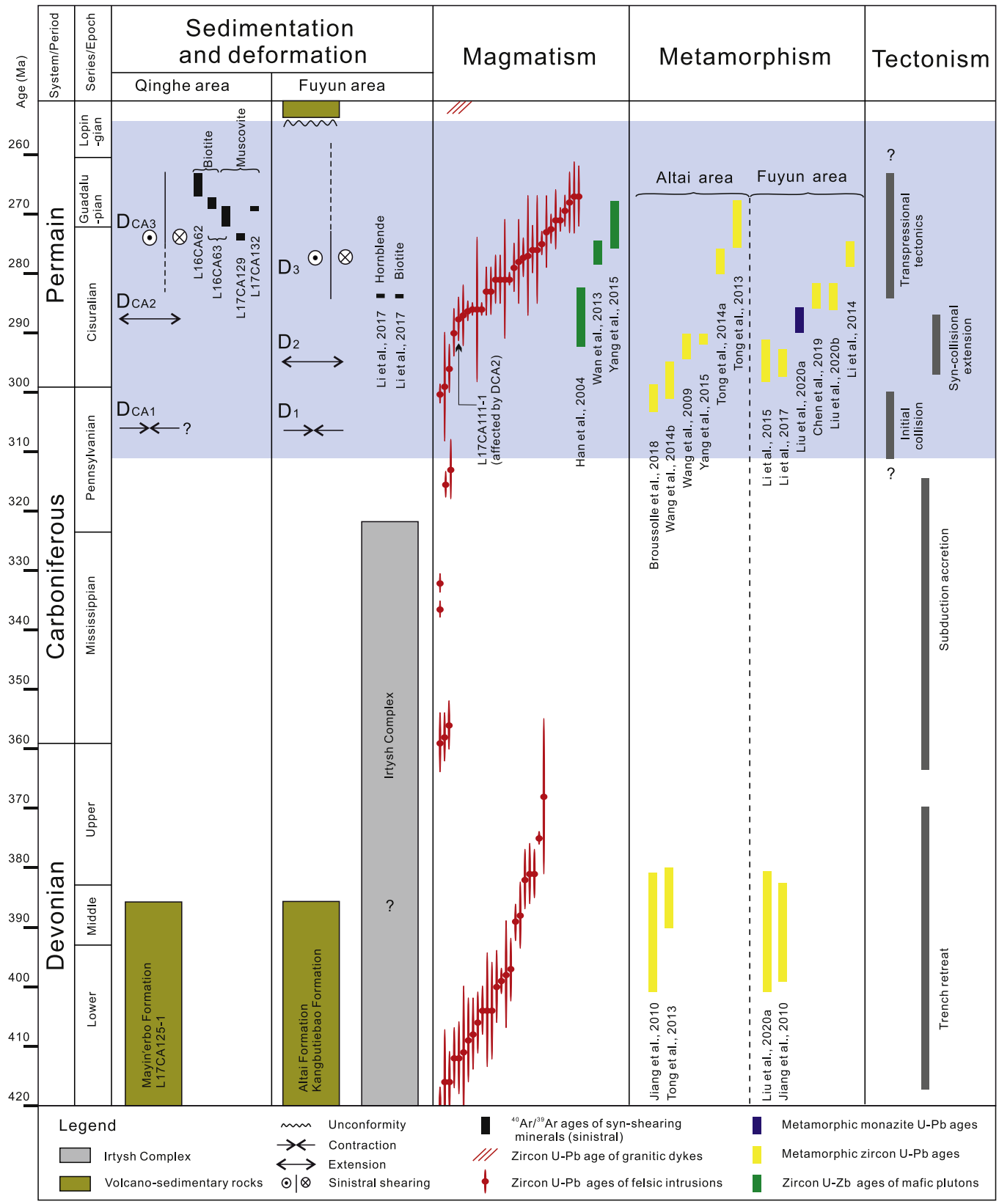


**Fig. 12.** Space-time diagram highlighting Devonian to Permian geological events in the southern Chinese Altai Orogen. Information on the deformation patterns and timing in the Fuyun area is from Li et al. (2015, 2017). Permian intrusive rocks in the northern Dulate Arc are also compiled. Ages of granitoids are from Han et al. (2006), Tong et al. (2006, 2014b and references therein), Wang et al. (2006), Yuan et al. (2007), Sun et al. (2008), Cai et al. (2011), and Zhang et al. (2012). For the ages and locations of high-temperature metamorphism (Wang et al., 2009b, 2014b; Tong et al., 2013, 2014a; Li et al., 2014, 2015, 2017; Yang et al., 2015; Broussolle et al., 2018; Chen et al., 2019; Liu et al., 2020b, 2020a) and Permian mafic intrusions (Han et al., 2006; Wan et al., 2013; Yang et al., 2015), see Fig. 1. $^{40}Ar/^{39}Ar$ ages refer only to those obtained from syn-shearing minerals. The length of the rectangles represents the error of the reported ages.

Junggar Terrane with the Chinese Altai Orogen was controlled by oblique convergence (Qu and Zhang, 1994; Laurent-Charvet et al., 2003; Li et al., 2015), whereas others proposed orthogonal convergence (Briggs et al., 2007, 2009; Hong et al., 2015). Models that suggested oblique convergence pointed out that during collision, the Irtysh Shear Zone was active as a large-scale strike-slip system that extended from northeastern Kazakhstan to northwestern China. Conversely, suggestions for orthogonal convergence have been supported by the dominant contractional deformation in the collisional zone and the idea that strike-slip shearing was limited to local zones that accommodated along-strike variations in the overall contractional deformation. Our structural and geochronological data from the Qinghe area indicate that sinistral shearing took place during the Permian along NW–SE mylonite zones (Fig. 2a). These shear zones are kinematically compatible with coeval NW–SE strike-slip shear zones farther west in the Fuyun area and northeastern Kazakhstan (Qu and Zhang, 1994; Laurent-Charvet et al., 2003; Buslov et al., 2004b; Glorie et al., 2012; Zhang et al., 2012; Li et al., 2015). It appears, therefore, that strike-slip deformation was not local, thus supporting the oblique convergence model for the period 283–265 Ma. Our structural observations also demonstrate that NW–SE $D_{CA3}$ folds in the southern Chinese Altai are sub-parallel to the sinistral mylonite zones (Fig. 2a and b), similar to observations from the Fuyun area (Figs. 1b and 12), which were interpreted to result from strain partitioning of transpressional deformation during oblique convergence (Fig. 13c; Li et al., 2015). Such an interpretation is supported by the simultaneous development of sinistral shearing and NW–SE $D_{CA3}$ folds along the southern Chinese Altai (Section 6.1). The pure-shear component of this transpression might have contributed to the fast exhumation along Mylonite Zone 1, as inferred from the overlapping $^{40}Ar/^{39}Ar$ biotite and muscovite ages (Section 6.1).

Our results show that two phases of folding ($D_{CA1}$ and $D_{CA2}$) affected rocks north of Mylonite Zone 1 prior to the occurrence of $D_{CA3}$ folds. $D_{CA1}$ was strongly transposed by the dominant $D_{CA2}$ fabric. The original orientation of the $S_{CA2}$ foliation was likely shallowly dipping, based on the observation that it was folded into shallowly plunging inclined $D_{CA3}$ folds (Fig. 3i). The hinges of these folds ($B_{CA32}$) are subparallel to the $L_{CA2}$ stretching lineation (Fig. 3i and j), which in turn, is sub-parallel to the strike of the Chinese Altai Orogen. Our geochronological results constrain the timing of $D_{CA2}$ to the Permian (post ~288 Ma), but the tectonic context of $D_{CA2}$ remains enigmatic. Similar shallowly dipping fabrics associated with orogen-parallel stretching lineations was also reported and dated in the Early Permian farther west in the Fuyun area, which were interpreted as evidence of orogen-parallel extension (Fig. 12; Li et al., 2015, 2017). If so, $D_{CA1}$ might represent an earlier contractional event associated with crustal thickening (Fig. 13a), which was followed by orogen-parallel extension ($D_{CA2}$; Fig. 13b).

During the Permian, the southern Chinese Altai Orogen experienced a thermal event that led to high-temperature metamorphism (Figs. 1 and 12; Wang et al., 2009b, 2014b; Tong et al., 2013, 2014a; Li et al., 2014; Li et al., 2015, 2017; Yang et al., 2015; Broussolle et al., 2018; Chen et al., 2019; Liu et al., 2020b, 2020a) and widespread magmatism (Fig. 12; Han et al., 2004; Wang et al., 2006; Yuan et al., 2007; Sun et al., 2008; Cai et al., 2011, 2012a; Zhang et al., 2012; Wan et al., 2013; Tong et al., 2014b and references therein; Yang et al., 2015). The timing of peak high-temperature metamorphism in the southern Chinese Altai Orogen has been constrained to ~301–272 Ma based on available monazite U–Th–Pb and zircon U–Pb ages (Figs. 1b and 12). A magmatic flare-up in the southern Chinese Altai Orogen also occurred during this period (Fig. 12; Tong et al., 2014b; Tang et al., 2017). Previous studies have suggested that this thermal event was generated by the Tarim mantle plume (Zhang et al., 2012; Xu et al., 2014; Liu et al., 2014), but the center of this plume was located >750 km from the southern Chinese Altai Orogen (Windley and Xiao, 2018). Furthermore, the types of igneous rocks (e.g., hornblende-bearing gabbro) found in the Chinese

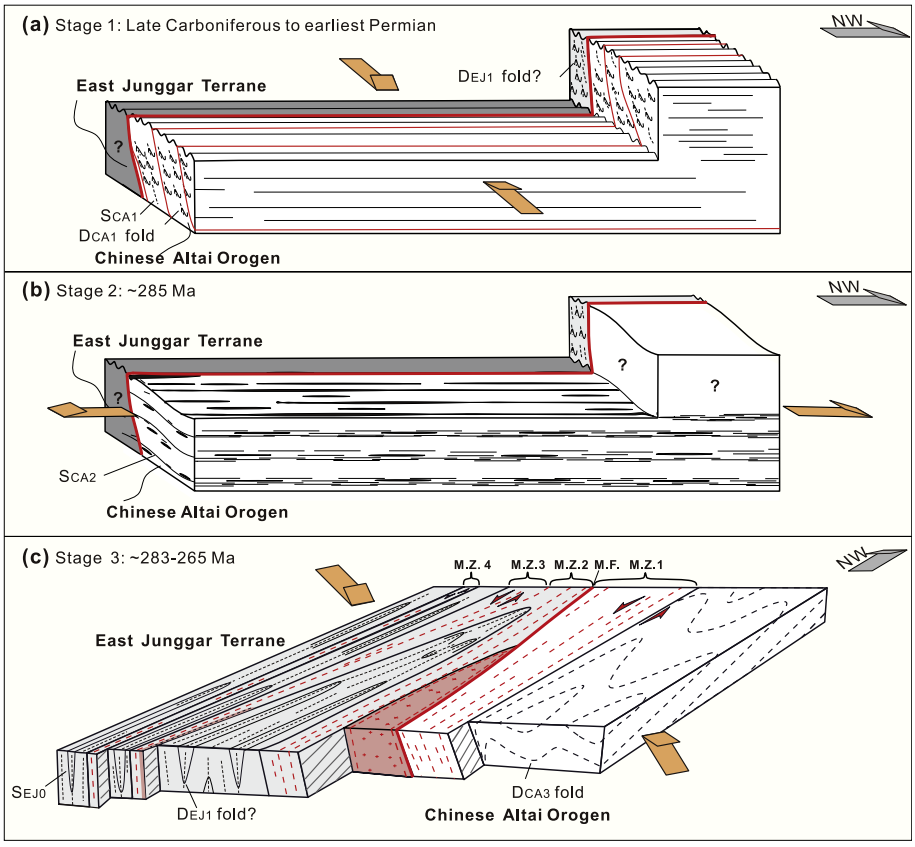


**Fig. 13.** Cartoon showing the three stages of collisional processes between the East Junggar Terrane and the Chinese Altai Orogen, following the closure of the Ob-Zaisan Ocean. Abbreviations: M.Z., Mylonite Zone; M.F., Mayin'erbo Fault.

Altai Orogen (Wan et al., 2013) are not compatible with a plume-derived magma from a deep anhydrous mantle source. Accordingly, it is unlikely that the Permian thermal even was related to a mantle plume. Alternatively, is possible that Permian high-temperature metamorphism and magmatism were associated with the thermal response to the collision of the East Junggar Terrane with the Chinese Altai Orogen (e.g. Li et al., 2014). This interpretation is supported by our structural observations, which show evidence of orogen-parallel extension ($D_{CA2}$) during the Early Permian (~288–283 Ma). This extensional episode could have led to mantle upwelling and an elevated thermal gradient.

Overall, our structural observations and geochronological data support the model for an oblique collision between the East Junggar Terrane and the Chinese Altai Orogen at 283–265 Ma (Fig. 13c). This stage of deformation was possibly preceded by an earlier collisional phase associated with crustal thickening ($D_{CA1}$; Fig. 13a) and orogenic extensional collapse ($D_{CA2}$; Fig. 13b). Syn-collisional extension might have been responsible for elevating the thermal gradient along the Irtysh Shear Zone. The role of steeply dipping NW–SE $D_{EJ1}$ fabric in the northern East Junggar Terrane (Fig. 2) remains poorly constrained, but was possibly linked to the earliest phase of collision (Fig. 13a). In the context of the whole western CAOB, our results support the suggestion that the buildup of this giant orogenic system involved the amalgamation of multiple arc systems (Xiao et al., 2004, 2010; Windley et al., 2007).

#### 6.2.3. *The larger-scale expression of the Irtysh Shear Zone*

The westward extension of the Irtysh Shear Zone in northeastern Kazakhstan is expressed by three strike-slip shear zones, which are, from north to south, the North-East Fault, the Irtysh Shear Zone, and the Char Shear Zone (Fig. 1a). These shear zones are associated with sinistral mylonitic fabrics, dated by $^{40}Ar/^{39}Ar$ geochronology to 283–265 Ma (Buslov et al., 2001, 2003; 2004a, 2004b; Travin et al., 2001; Vladimirov et al., 2008; Zhang et al., 2012). These strike-slip structures and geochronological constraints are consistent with the evidence from Qinghe and Fuyun areas in northwestern China (Fig. 12), thus supporting the suggestion that the southwestern margin of the peri-Siberian orogenic system was affected by large-scale sinistral strike-slip deformation during the Early–Middle Permian (Figs. 1a and 14).

In northeastern Kazakhstan, the suture between the peri-Siberian and Kazakhstan orogenic systems is represented by the Char Shear Zone (Fig. 1a; Şengör et al., 1993; Buslov et al., 2004b; Safonova, 2014; Safonova et al., 2018). Evidence supporting the suggestion that the Char Shear Zone is a major late Paleozoic suture includes: (1) the widespread occurrence of ophiolitic rocks along this shear zone (Wang et al., 2012; Safonova et al., 2018); (2) the recognition that magmatic rocks along the Char Shear Zone changed from subduction-related to collision-related during the Late Carboniferous (Kuibida et al., 2016, 2019; Safonova et al., 2018; Khromykh et al., 2019); and (3) the abrupt change across the shear zone in detrital zircon age populations derived from pre-Permian sedimentary rocks (Li et al., 2017). An alternative interpretation, proposed by Buslov (2011) and Buslov et al. (2019), postulated that the peri-Siberian and Kazakhstan orogenic systems might represent a consolidated collage in the early Paleozoic. This model, which implies that late Paleozoic deformation in northeastern Kazakhstan was entirely intracontinental, seems at odds with our interpretation for the plate tectonic processes in northwestern China. We emphasize, however, that due to the presence of Meso–Cenozoic cover sediments of the Junggar Basin (Fig. 1), it is difficult to test whether the late Paleozoic convergence history of the East Junggar Terrane (this study; Fig. 13) is also applicable to the West Junggar Terrane (and its extension in northeastern Kazakhstan).

On the scale of the whole western CAOB, the sinistral Irtysh Shear Zone (and related structures in northeastern Kazakhstan) might be kinematically linked to a series of dextral shear zones that occur farther south (Fig. 1a). Activity along these dextral shear zones took place at ~290–240 Ma (Shu et al., 1999; Laurent-Charvet et al., 2003; Lin et al., 2009; Wang et al., 2009a; Cai et al., 2012b; Konopelko et al., 2013; Han and Zhao, 2018; Li et al., 2020b). It appears, therefore, that NW–SE shear zones in the northern and southern parts of the western CAOB were subjected simultaneously to sinistral and dextral shearing, respectively. The combined effect of this deformation allowed an eastward migration of orogenic components (e.g., East Junggar Terrane; Fig. 14), possibly in response to the convergence of the Siberian, Baltic and Tarim cratons during the Permian (Wang et al., 2008; Li et al., 2015). The strike-slip deformation also overlaps in time with the occurrence of Permian extensional basins (e.g., Tuha Basin, Fig. 1a) that were interpreted by Allen et al. (1995) and Wartes et al. (2002) to be pull-apart basins associated with the development of shear zones.

## 7. Conclusions

Our structural observations and $^{40}Ar/^{39}Ar$ results from the eastern

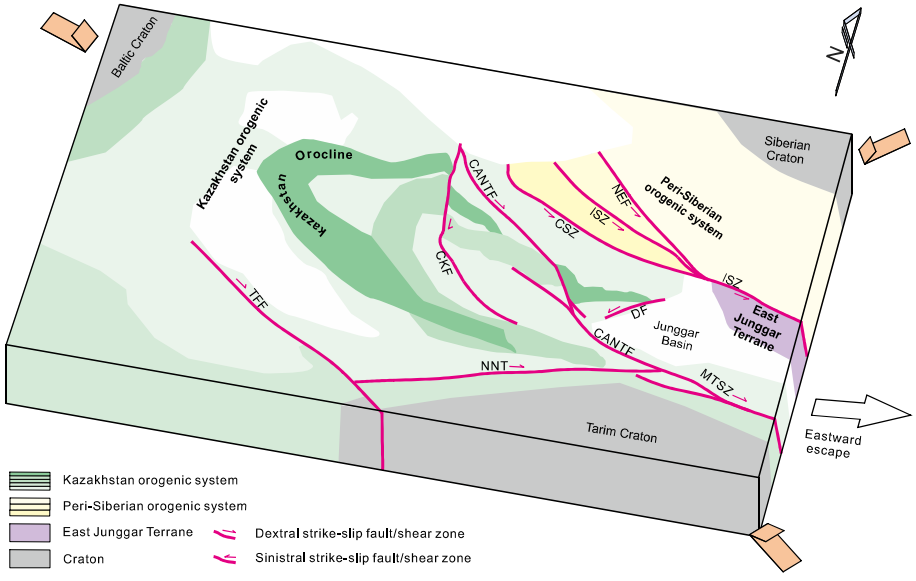


**Fig. 14.** Block diagram illustrating Permian strike-slip shear zones in the western CAOB. The variable kinematics from north to south suggests an eastward escape of orogenic material (after Li et al., 2015). See Fig. 1a for abbreviations.

segment of the Irtysh Shear Zone (Qinghe area) show that four NW–SE sinistral mylonite zones were active at 283–265 Ma. Domains bounded by these mylonite zones were subjected to folding. Three generations of folds were recognized in the southern Chinese Altai Orogen ($D_{CA1}$–$D_{CA3}$). The earliest fabric ($S_{CA1}$) is recognized locally and is strongly transposed by the dominant fabric ($S_{CA2}$). $S_{CA2}$ foliation is associated with a shallowly plunging stretching lineation ($L_{CA2}$) trending NW–SE parallel to the orogenic strike. We infer that the orientation of $S_{CA2}$ was shallowly dipping prior to the development of NW–SE inclined $D_{CA3}$ folds, which are characterized by shallowly plunging hinges sub-parallel to the $L_{CA2}$ stretching lineations. These deformation structures were developed simultaneously with the collision between the East Junggar Terrane and the Chinese Altai Orogen. Combined with our new zircon data, the timing of this collision can be constrained to the Late Carboniferous and Permian. During the Early–Middle Permian, the collision was oblique, as suggested by the evidence of sinistral shearing and $D_{CA3}$ folding. The earlier collisional phases involved orogenic thickening ($D_{CA1}$) and orogen-parallel extension ($D_{CA2}$), with the latter being responsible for Permian high-temperature metamorphism and granitic magmatism. On a larger scale, the sinistral Irtysh Shear Zone extends into northeastern Kazakhstan. Combined with dextral shearing farther south, deformation was responsible for transferring material eastwards, possibly in response to the Permian convergence of the Siberian, Baltic and Tarim cratons.

## Declaration of competing interest

The authors declare that they have no known competing financial interests or personal relationships that could have appeared to influence the work reported in this paper.

## Acknowledgments

This study was financially supported by the National Natural Science Foundation of China (41872222), the National Key Research and Development Program of China (Grant No. 2017YFC0601205), the international partnership program of the Chinese Academy of Sciences (Grant No. 132744KYSB20190039), and Hong Kong Research Grant Council (HKU17302317 and HKU17303415). P. Li acknowledges the Thousand Youth Talents Plan, and a project from Guangdong Province (2019QN01H101). G.R acknowledges funding through the Chinese Academy of Science President's International Fellowship (2020VCB0005). Y. Jiang acknowledges the Guangdong Special Support Program. We thank Karel Schulmann for many constructive discussions on the tectonics of the Altai Mountains, and Xiangsong Wang, Jiaqi Ling and Huiming Huang for their assistance during field work. The manuscript benefits from comments by Mark Allen and an anonymous reviewer. This is a contribution of GIGCAS (No.IS-2886), the Chemical Geodynamics Joint Laboratory between Hong Kong University and GIG (CAS) as well as IGCP 662.

## Appendices A, B and C. Supplementary data

Supplementary data associated with this article can be found, in the online version, at https://doi.org/10.1016/j.jsg.2020.104126.

## References

Allen, M.B., Şengör, A.M.C., Natalin, B.A., 1995. Junggar, Turfan and Alakol basins as late Permian to ?early triassic extensional structures in a sinistral shear zone in the Altaid orogenic collage, central Asia. J. Geol. Soc. 152, 327–338.

BGMRX, 1972. Geological Map and Explanatory Note of the Ertai Sheet: BGMRX, Scale 1: 200,000. Geological Publishing House, Beijing.

Briggs, S.M., Yin, A., Manning, C.E., Chen, Z.L., Wang, X.F., Grove, M., 2007. Late Paleozoic tectonic history of the Ertix fault in the Chinese Altai and its implications for the development of the central Asian orogenic system. Geol. Soc. Am. Bull. 119, 944–960.

Briggs, S.M., Yin, A., Manning, C.E., Chen, Z.L., Wang, X.F., 2009. Tectonic development of the southern Chinese Altai Range as determined by structural geology, thermobarometry, $^{40}Ar/^{39}Ar$ thermochronology, and Th/Pb ion-microprobe monazite geochronology. Geol. Soc. Am. Bull. 121, 1381–1393.

Broussolle, A., Aguilar, C., Sun, M., Schulmann, K., Stipska, P., Jiang, Y.D., Yu, Y., Xiao, W.J., Wang, S., Mikova, J., 2018. Polycyclic Palaeozoic evolution of accretionary orogenic wedge in the southern Chinese Altai: evidence from structural relationships and U-Pb geochronology. Lithos 314, 400–424.

Buslov, M.M., Saphonova, I.Y., Watanabe, T., Obut, O.T., Fujiwara, Y., Iwata, K., Semakov, N.N., Sugai, Y., Smirnova, L.V., Kazansky, A.Y., 2001. Evolution of the Paleo-Asian ocean (Altai-Sayan region, central Asia) and collision of possible Gondwana-derived terranes with the southern marginal part of the Siberian continent. Geosci. J. 5, 203–224.

Buslov, M.M., Watanabe, T., Smirnova, L.V., Fujiwara, I., Iwata, K., de Grave, I., Semakov, N.N., Travin, A.V., Kir'yanova, A.P., Kokh, D.A., 2003. Role of strike-slip faults in Late Paleozoic-Early Mesozoic tectonics and geodynamics of the Altai-Sayan and East Kazakhstan folded zone. Russ. Geol. Geophys. 44, 49–75 in Russian with the English abstract.

Buslov, M.M., Cai, K., Abildaeva, M.A., 2019. Late Paleozoic tectonics of the Junggar-Altai–Sayan Foldbelt. IOP Conf. Ser.: Earth Environ. Sci. 319, 1–6.

Buslov, M.M., Fujiwara, Y., Iwata, K., Semakov, N., 2004a. Late Paleozoic-early mesozoic geodynamics of central Asia. Gondwana Res. 7, 791–808.

Buslov, M.M., Watanabe, T., Fujiwara, Y., Iwata, K., Smirnova, L.V., Safonova, I.Y., Semakov, N.N., Kiryanova, A.P., 2004b. Late Paleozoic faults of the Altai region, Central Asia: tectonic pattern and model of formation. J. Asian Earth Sci. 23, 655–671.

Buslov, M.M., 2011. Tectonics and geodynamics of the central Asian Foldbelt: the role of late Paleozoic large-amplitude strike-slip faults. Russ. Geol. Geophys. 52, 52–71.

Cai, K.D., Sun, M., Yuan, C., Zhao, G.C., Xiao, W.J., Long, X.P., Wu, F.Y., 2011. Prolonged magmatism, juvenile nature and tectonic evolution of the Chinese Altai, NW China: evidence from zircon U–Pb and Hf isotopic study of Paleozoic granitoids. J. Asian Earth Sci. 42, 949–968.

Cai, K.D., Sun, M., Yuan, C., Xiao, W.J., Zhao, G.C., Long, X.P., Wu, F.Y., 2012a. Carboniferous mantle-derived felsic intrusion in the Chinese Altai, NW China: implications for geodynamic change of the accretionary orogenic belt. Gondwana Res. 22, 681–698.

Cai, Z.H., Xu, Z.Q., He, B.Z., Wang, R.R., 2012b. Age and tectonic evolution of ductile shear zones in the eastern Tianshan-Beishan orogenic belt. Acta Petrol. Sin. 28, 1875–1895 in Chinese with the English abstract.

Cao, S.Y., Neubauer, F., 2016. Deep crustal expressions of exhumed strike-slip fault systems: Shear zone initiation on rheological boundaries. Earth Sci. Rev. 162, 155–176.

Chen, M., Sun, M., Li, P.F., Zheng, J.P., Cai, K.D., Su, Y.P., 2019. Late Paleozoic accretionary and collisional processes along the southern peri-Siberian orogenic system: new constraints from amphibolites within the Irtysh complex of Chinese Altai. J. Geol. 127, 241–262.

Glorie, S., De Grave, J., Delvaux, D., Buslov, M.M., Zhimulev, F.I., Vanhaecke, F., Elburg, M.A., Van den Haute, P., 2012. Tectonic history of the Irtysh shear zone (NE Kazakhstan): new constraints from zircon U/Pb dating, apatite fission track dating and palaeostress analysis. J. Asian Earth Sci. 45, 138–149.

Han, B.F., Ji, J.Q., Song, B., Chen, L.H., Li, Z., 2004. SHRIMP zircon U–Pb ages of Kalatongke No. 1 and Huangshandong Cu–Ni-bearing mafic–ultramafic complexes, North Xinjiang, and geological implications. Chin. Sci. Bull. 49, 2424–2429 in Chinese with the English abstract.

Han, B.F., Ji, J.Q., Song, B., Chen, L.H., Zhang, L., 2006. Late Paleozoic vertical growth of continental crust around the Junggar Basin, Xinjiang, China (part I): timing of post-collisional plutonism. Acta Petrol. Sin. 22, 1077–1086 in Chinese with the English abstract.

Han, Y.G., Zhao, G.C., 2018. Final amalgamation of the Tianshan and Junggar orogenic collage in the southwestern central Asian orogenic belt: constraints on the closure of the Paleo-Asian ocean. Earth Sci. Rev. 186, 129–152.

He, G.Q., Han, B.F., Yue, Y.J., Wang, J.Y., 1990. Tectonic division and crustal evolution of Altay orogenic belt in China. Geosci. Xinjiang 2, 9–20 in Chinese with the English abstract.

Hong, T., Xiang, P., You, J., Zhang, L.C., Wu, C., Wu, Q., Xu, X.W., 2015. Texture and formation age of the eastern Irtysh collision belt. Acta Petrol. Sin. 31 (2), 571–593 in Chinese with the English abstract.

Hong, T., Klemd, R., Gao, J., Xiang, P., Xu, X.W., You, J., Wang, X.S., Wu, C., Li, H., Ke, Q., 2017. The tectonic evolution of the Irtysh tectonic belt: new zircon U–Pb ages of arc-related and collisional granitoids in the Kalaxiangar tectonic belt, NW China. Lithos 272–273, 46–68.

Jahn, B.M., 2004. The central Asian orogenic belt and growth of the continental crust in the Phanerozoic. Geol. Soc. Lond. Spec. Publ. 226, 73–100.

Jiang, Y.D., Sun, M., Zhao, G.C., Yuan, C., Xiao, W.J., Xia, X.P., Long, X.P., Wu, F.Y., 2010. The similar to 390 Ma high-T metamorphic event in the Chinese Altai: a consequence of ridge-subduction? Am. J. Sci. 310, 1421–1452.

Jiang, Y.D., Sun, M., Zhao, G.C., Yuan, C., Xiao, W.J., Xia, X.P., Long, X.P., Wu, F.Y., 2011. Precambrian detrital zircons in the Early Paleozoic Chinese Altai: their provenance and implications for the crustal growth of central Asia. Precambrian Res. 189, 140–154.

Jiang, Y.D., Štípská, P., Sun, M., Schulmann, K., Zhang, J., Wu, Q.H., Long, X.P., Yuan, C., Racek, M., Zhao, G.C., Xiao, W.J., 2015. Juxtaposition of Barrovian and migmatite domains in the Chinese Altai: a result of crustal thickening followed by doming of partially molten lower crust. J. Metamorph. Geol. 33, 45–70.

Jiang, Y.D., Schulmann, K., Sun, M., Weinberg, R.F., Stipska, P., Li, P.F., Zhang, J., Chopin, F., Wang, S., Xia, X.P., Xiao, W.J., 2019. Structural and geochronological

constraints on Devonian suprasubduction tectonic switching and Permian collisional dynamics in the Chinese Altai, central Asia. Tectonics 38, 253–280.
Khromykh, S.V., Izokh, A.E., Gurova, A.V., Cherdantseva, M.V., Savinsky, I.A., Vishnevsky, A.V., 2019. Syncollisional gabbro in the Irtysh shear zone, Eastern Kazakhstan: compositions, geochronology, and geodynamic implications. Lithos 346–347. https://doi.org/10.1016/j.lithos.2019.07.011.
Konopelko, D., Seltmann, R., Apayarov, F., Belousova, E., Izokh, A., Lepekhina, E., 2013. U–Pb–Hf zircon study of two mylonitic granite complexes in the Talas-Fergana fault zone, Kyrgyzstan, and Ar–Ar age of deformations along the fault. J. Asian Earth Sci. 73, 334–346.
Koppers, A.A.P., 2002. ArArCALC-Software for Ar-40/Ar-39 age calculations. Comput. Geosci. 28, 605–619.
Kuibida, M.L., Safonova, I.Y., Yermolov, P.V., Vladimirov, A.G., Kruk, N.N., Yamamoto, S., 2016. Tonalites and plagiogranites of the Char suture-shear zone in East Kazakhstan: implications for the Kazakhstan-Siberia collision. Geosci. Front. 7, 141–150.
Kuibida, M.L., Dyachkov, B.A., Vladimirov, A.G., Kruk, N.N., Khromykh, S.V., Kotler, P. D., Rudnev, S.N., Kruk, E.A., Kuibida, Y.V., Oitseva, T., 2019. Contrasting granitic magmatism of the Kalba fold belt (East Kazakhstan): evidence for Late Paleozoic post-orogenic events. J. Asian Earth Sci. 175, 178–198.
Langille, J.M., Jessup, M.J., Cottle, J.M., Newell, D., Seward, G., 2010. Kinematic evolution of the Ama Drime detachment: insights into orogen-parallel extension and exhumation of the Ama Drime Massif, Tibet–Nepal. J. Struct. Geol. 32, 900–919.
Laurent-Charvet, S., Charvet, J., Shu, L.S., Ma, R.S., Lu, H.F., 2002. Palaeozoic late collisional strike-slip deformations in Tianshan and Altay, eastern Xinjiang, NW China. Terra. Nova 14, 249–256.
Laurent-Charvet, S., Charvet, J., Monié, P., Shu, L.S., 2003. Late Paleozoic strike-slip shear zones in eastern central Asia (NW China): new structural and geochronological data. Tectonics 22. https://doi.org/10.1029/2001TC901047.
Li, D., He, D.F., Sun, M., Zhang, L., 2020a. The role of arc-arc collision in accretionary orogenesis: insights from ~320 Ma tectono-sedimentary Transition in the Karamaili area, NW China. Tectonics 39. https://doi.org/10.1029/2019TC005623.
Li, P.F., Sun, M., Rosenbaum, G., Cai, K.D., Yu, Y., 2015. Structural evolution of the Irtysh shear zone (northwestern China) and implications for the amalgamation of arc systems in the central Asian orogenic belt. J. Struct. Geol. 80, 142–156.
Li, P.F., Sun, M., Rosenbaum, G., Cai, K.D., Chen, M., He, Y.L., 2016a. Transpressional deformation, strain partitioning and fold superimposition in the southern Chinese Altai, Central Asian Orogenic Belt. J. Struct. Geol. 87, 64–80.
Li, P.F., Sun, M., Rosenbaum, G., Jiang, Y.D., Cai, K.D., 2016b. Structural evolution of zonal metamorphic sequences in the southern Chinese Altai and relationships to Permian transpressional tectonics in the Central Asian Orogenic Belt. Tectonophysics 693, 277–289.
Li, P.F., Sun, M., Rosenbaum, G., Jourdan, F., Li, S.Z., Cai, K.D., 2017. Late Paleozoic closure of the Ob-Zaisan Ocean along the Irtysh shear zone (NW China): implications for arc amalgamation and oroclinal bending in the Central Asian orogenic belt. Geol. Soc. Am. Bull. 129, 547–569.
Li, P.F., Sun, M., Rosenbaum, G., Yuan, C., Safonova, I., Cai, K.D., Jiang, Y.D., Zhang, Y. Y., 2018. Geometry, kinematics and tectonic models of the Kazakhstan Orocline, Central Asian Orogenic Belt. J. Asian Earth Sci. 153, 42–56.
Li, P.F., Sun, M., Shu, C.T., Yuan, C., Jiang, Y.D., Zhang, L., Cai, K.D., 2019. Evolution of the central Asian orogenic belt along the Siberian margin from neoproterozoic-early Paleozoic accretion to Devonian trench retreat and a comparison with Phanerozoic eastern Australia. Earth Sci. Rev. 198 https://doi.org/10.1016/j.earscirev.2019.102951.
Li, P.F., Sun, M., Rosenbaum, G., Cai, K.D., Yuan, C., Jourdan, F., Xia, X.P., Jiang, Y.D., Zhang, Y.Y., 2020b. Tectonic Evolution of the Chinese Tianshan Orogen from Subduction to Arc-Continent Collision: Insight from Polyphase Deformation along the Gangou Section. Geological Society of America Bulletin, Central Asia (in press).
Li, Z.L., Yang, X.Q., Li, Y.Q., Santosh, M., Chen, H.L., Xiao, W.J., 2014. Late Paleozoic tectono–metamorphic evolution of the Altai segment of the Central Asian Orogenic Belt: constraints from metamorphic P–T pseudosection and zircon U–Pb dating of ultra-high-temperature granulite. Lithos 204, 83–96.
Liang, P., Chen, H.Y., Hollings, P., Wu, C., Xiao, B., Bao, Z.W., Xu, D., 2016. Geochronology and geochemistry of igneous rocks from the Laoshankou District, north Xinjiang: implications for the late Paleozoic tectonic evolution and metallogenesis of East Junggar. Lithos 266–267, 115–132.
Lin, W., Faure, M., Shi, Y., Wang, Q., Li, Z., 2009. Palaeozoic tectonics of the south-western Chinese Tianshan: new insights from a structural study of the high-pressure/low-temperature metamorphic belt. Int. J. Earth Sci. 98, 1259–1274.
Liu, F., Lin, W., Chen, K., Jiang, L., Wang, Q.C., 2013. Structural deformation and significance of Erqis fault zone in southern margin of Chinese Altay Orogen. Acta Petrol. Sin. 29, 1811–1824 in Chinese with the English abstract.
Liu, H.Q., Xu, Y.G., Tian, W., Zhong, Y.T., Mundil, R., Li, X.H., Yang, Y.H., Luo, Z.Y., Shang-Guan, S.M., 2014. Origin of two types of rhyolites in the Tarim Large Igneous Province: consequences of incubation and melting of a mantle plume. Lithos 204, 59–72.
Liu, Y.S., Hu, Z.C., Zong, K.Q., Gao, C.G., Gao, S., Xu, J.A., Chen, H.H., 2010. Reappraisement and refinement of zircon U-Pb isotope and trace element analyses by LA-ICP-MS. Chin. Sci. Bull. 55, 1535–1546.
Liu, Z., Bartoli, O., Tong, L.X., Xu, Y.G., Gianola, O., Li, C., 2020a. Anatexis and metamorphic history of Permian pelitic granulites from the southern Chinese Altai: constraints from petrology, melt inclusions and phase equilibria modelling. Lithos 360–361, 1–16.
Liu, Z., Bartoli, O., Tong, L.X., Xu, Y.G., Huang, X.L., 2020b. Permian ultrahigh–temperature reworking in the southern Chinese Altai: evidence from petrology, P–T estimates, zircon and monazite U–Th–Pb geochronology. Gondwana Res. 78, 20–40.
Long, X.P., Sun, M., Yuan, C., Xiao, W.J., Lin, S.F., Wu, F.Y., Xia, X.P., Cai, K.D., 2007. Detrital zircon age and Hf isotopic studies for metasedimentary rocks from the Chinese Altai: implications for the early Paleozoic tectonic evolution of the central Asian orogenic belt. Tectonics 26. https://doi.org/10.1029/2007TC002128.
Long, X.P., Sun, M., Yuan, C., Xiao, W.J., Cai, K.D., 2008. Early Paleozoic sedimentary record of the Chinese Altai: implications for its tectonic evolution. Sediment. Geol. 208, 88–100.
Ludwig, K.R., 2003. Isoplot 3.00: A Geochronological Toolkit for Microsoft Excel. Berkeley Geochronology Center Special Publication.
Nie, F., Tian, X., Li, Z., 2014. Age and provenance of the original Devonian in the eastern Junggar orogenic belt: the evidence of detrital zircon U-Pb geochronology. Chin. J. Geol. 49, 695–717 in Chinese with the English abstract.
Ohara, K.D., Yang, X.Y., Xie, G.Y., Li, Z.C., 1997. Regional δ18O gradients and fluid-rock interaction in the Altay accretionary complex, northwest China. Geology 25, 443–446.
Passchier, C.W., Trouw, R.A.J., 2005. Microtectonics. Springer, Berlin, Heidelberg, New York, pp. 102–108.
Qin, Y.X., Dong, Z.Y., Zhang, F.Z., 1991. Irtys-Mayinebe fault belt: an important tectonic coalescence zone. Bull. Nanjing Inst. Geol. Min. Resour. Chin. Acad. Geosci. 12, 69–76 in Chinese with the English abstract.
Qu, G.S., Zhang, J.J., 1991. Irtysh structural zone. Geosci. Xinjiang 3, 115–131 in Chinese with the English abstract.
Qu, G.S., Zhang, J.J., 1994. Oblique thrust systems in the Altay orogen, China. J. Southeast Asian Earth Sci. 9, 277–287.
Renne, P.R., Balco, G., Ludwig, K.R., Mundil, R., Min, K., 2011. Joint determination of K-40 decay constants and Ar-40*/K-40 for the Fish Canyon sanidine standard, and improved accuracy for Ar-40/Ar-39 geochronology. Response to the comment by W. H. Schwarz et al. on Geochem. Cosmochim. Acta 75, 5097–5100. by PR Renne et al. (2010).
Safonova, I., 2014. The Russian-Kazakh Altai orogen: an overview and main debatable issues. Geosci. Front. 5, 537–552.
Safonova, I., Komiya, T., Romer, R.L., Simonov, V., Seltmann, R., Rudnev, S., Yamamoto, S., Sun, M., 2018. Supra-subduction igneous formations of the Char ophiolite belt, East Kazakhstan. Gondwana Res. 59, 159–179.
Sanderson, D.J., Marchini, W., 1984. Transpression. J. Struct. Geol. 6, 449–458.
Scibiorski, E., Tohver, E., Jourdan, F., 2015. Rapid cooling and exhumation in the western part of the mesoproterozoic Albany-Fraser orogen, western Australia. Precambrian Res. 265, 232–248.
Şengör, A.M.C., Natal'in, B.A., 1996. Turkic-type orogeny and its role in the making of the continental crust. Annu. Rev. Earth Planet Sci. 24, 263–337.
Şengör, A.M.C., Natal'in, B.A., Burtman, V.S., 1993. Evolution of the Altaid tectonic collage and Paleozoic crustal growth in Eurasia. Nature 364, 299–307.
Shu, L.S., Charvet, J., Guo, L.Z., Lu, H.F., Laurent-Charvet, S., 1999. A large-scale Palaeozoic dextral ductile strike-slip zone: the Aqqikkudug-Weiya zone along the northern margin of the Central Tianshan belt, Xinjiang, NW China. Acta Geol. Sin. Engl. Ed. 73, 148–162.
Sláma, J., Košler, J., Condon, D.J., Crowley, J.L., Gerdes, A., Hanchar, J.M., Horstwood, M.S.A., Morris, G.A., Nasdala, L., Norberg, N., Schaltegger, U., Schoene, B., Tubrett, M.N., Whitehouse, M.J., 2008. Plešovice zircon-A new natural reference material for U–Pb and Hf isotopic microanalysis. Chem. Geol. 249, 1–35.
Stipp, M., Stunitz, H., Heilbronner, R., Schmid, S.M., 2002. The eastern Tonale fault zone: a 'natural laboratory' for crystal plastic deformation of quartz over a temperature range from 250 to 700 degrees C. J. Struct. Geol. 24, 1861–1884.
Sun, M., Yuan, C., Xiao, W.J., Long, X.P., Xia, X.P., Zhao, G.C., Lin, S.F., Wu, F.Y., Kroner, A., 2008. Zircon U-Pb and Hf isotopic study of gneissic rocks from the Chinese Altai: Progressive accretionary history in the early to middle Palaeozoic. Chem. Geol. 247, 352–383.
Tang, G.J., Chung, S.L., Hawkesworth, C.J., Cawood, P.A., Wang, Q., Wyman, D.A., Xu, Y.G., Zhao, Z.H., 2017. Short episodes of crust generation during protracted accretionary processes: evidence from Central Asian Orogenic Belt, NW China. Earth Planet Sci. Lett. 464, 142–154.
Tong, L.X., Chen, Y.B., Xu, Y.G., Zhou, X., Liu, Z., 2013. Zircon U–Pb ages of the ultrahigh-temperature metapelitic granulite from the Altai orogeny, NW China, and geological implications. Acta Petrol. Sin. 29, 3435–3445 in Chinese with the English abstract.
Tong, L.X., Xu, Y.G., Cawood, P.A., Zhou, X., Chen, Y.B., Liu, Z., 2014a. Anticlockwise P-T evolution at ~280Ma recorded from ultrahigh-temperature metapelitic granulite in the Chinese Altai orogenic belt, a possible link with the Tarim mantle plume? J. Asian Earth Sci. 94, 1–11.
Tong, Y., Wang, T., Kovach, V.P., Hong, D.W., Han, B.F., 2006. Age and origin of the Takeshiken Postorogenic alkali-rich intrusive rocks in southern Altai, near the Mongolian border in China and its implications for continental growth. Acta Petrol. Sin. 22, 1267–1278 in Chinese with the English abstract.
Tong, Y., Wang, T., Siebel, W., Hong, D.W., Sun, M., 2012. Recognition of early Carboniferous alkaline granite in the southern Altai orogen: post-orogenic processes constrained by U-Pb zircon ages, Nd isotopes, and geochemical data. Int. J. Earth Sci. 101, 937–950.
Tong, Y., Wang, T., Jahn, B.M., Sun, M., Hong, D.W., Gao, J.F., 2014b. Post-accretionary Permian granitoids in the Chinese Altai orogen; geochronology, petrogenesis and tectonic implications. Am. J. Sci. 314, 80–109.
Travin, A.V., Boven, A., Plotnikov, A.V., Vladimirov, V.G., Theunissen, K., Vladimirov, A. G., Melnikov, A.I., Titov, A.V., 2001. $^{40}Ar/^{39}Ar$ dating of ductile deformations in the Irtysh shear zone, eastern Kazakhstan. Geochem. Int. 12, 1237–1241 in Russian.

Vladimirov, A.G., Kruk, N.N., Khromykh, S.V., Polyansky, O.P., Chervov, V.V., Vladimirov, V.G., Travin, A.V., Babin, G.A., Kuibida, M.L., Vladimirov, V.D., 2008. Permian magmatism and lithospheric deformation in the Altai caused by crustal and mantle thermal processes. Russ. Geol. Geophys. 49, 468–479.
Wan, B., Xiao, W.J., Windley, B.F., Yuan, C., 2013. Permian hornblende gabbros in the Chinese Altai from a subduction-related hydrous parent magma, not from the Tarim mantle plume. Lithos 5, 290–299.
Wang, B., Cluzel, D., Shu, L., Faure, M., Charvet, J., Chen, Y., Meffre, S., De Jong, K., 2009a. Evolution of calc-alkaline to alkaline magmatism through Carboniferous convergence to Permian transcurrent tectonics, western Chinese Tianshan. Int. J. Earth Sci. 98, 1275–1298.
Wang, T., Hong, D.W., Jahn, B.M., Tong, Y., Wang, Y.B., Han, B.F., Wang, X.X., 2006. Timing, petrogenesis, and setting of Paleozoic synorogenic intrusions from the Altai Mountains, northwest China: implications for the Tectonic evolution of an accretionary orogen. J. Geol. 114, 735–751.
Wang, T., Tong, Y., Li, S., Zhang, J.J., Shi, X.X., Li, J.Y., Han, B.F., Hong, D.W., 2010. Spatial and temporal variations of granitoids in the Altay orogen and their implications for tectonic setting and crustal growth:perspectives from Chinese Altay. Acta Petrol. Mineral. 29, 595–618 in Chinese with the English abstract.
Wang, T., Jahn, B.M., Kovach, V.P., Tong, Y., Wilde, S.A., Hong, D.W., Li, S., Salnikova, E.B., 2014a. Mesozoic intraplate granitic magmatism in the Altai accretionary orogen, NW China:implications for the orogenic architecture and crustal growth. Am. J. Sci. 314, 1–42.
Wang, W., Wei, C., Wang, T., Lou, Y., Chu, H., 2009b. Confirmation of pelitic granulite in the Altai orogen and its geological significance. Chin. Sci. Bull. 54, 2543–2548.
Wang, W., Wei, C.J., Zhang, Y.H., Chu, H., Zhao, Y., Liu, X.C., 2014b. Age and origin of sillimanite schist from the Chinese Altai metamorphic belt: implications for late Palaeozoic tectonic evolution of the Central Asian Orogenic Belt. Int. Geol. Rev. 56, 224–236.
Wang, Y., Li, J.Y., Sun, G.H., 2008. Postcollisional eastward extrusion and tectonic exhumation along the eastern Tianshan orogen, central Asia: constraints from dextral strike-slip motion and $^{40}Ar/^{39}Ar$ geochronological evidence. J. Geol. 116, 599–618.
Wang, Y.J., Long, X.P., Wilde, S.A., Xu, H.L., Sun, M., Xiao, W.J., Yuan, C., Cai, K.D., 2014c. Provenance of early Paleozoic metasediments in the central Chinese Altai: implications for tectonic affinity of the Altai-Mongolia terrane in the central Asian orogenic belt. Lithos 210, 57–68.
Wang, Y.W., Wang, J.B., Wang, L.J., Long, L.L., Tang, P.Z., Liao, Z., Zhang, H.Q., Shi, Y., 2012. The Tuerkubantao ophiolite mélange in Xinjiang, NW China: new evidence for the Erqis suture zone. Geosci. Front. 3, 587–602.
Wartes, M.A., Carroll, A.R., Greene, T.J., 2002. Permian sedimentary record of the Turpan-Hami basin and adjacent regions, northwest China: constraints on postamalgamation tectonic evolution. Geol. Soc. Am. Bull. 114, 131–152.
Wilhem, C., Windley, B.F., Stampfli, G.M., 2012. The Altaids of Central Asia: a tectonic and evolutionary innovative review. Earth Sci. Rev. 113, 303–341.
Windley, B.F., Kroner, A., Guo, J.H., Qu, G.S., Li, Y.Y., Zhang, C., 2002. Neoproterozoic to Paleozoic geology of the Altai orogen, NW China: new zircon age data and tectonic evolution. J. Geol. 110, 719–737.
Windley, B.F., Alexeiev, D., Xiao, W.J., Kröner, A., Badarch, G., 2007. Tectonic models for accretion of the central Asian orogenic belt. J. Geol. Soc. 164, 31–47.
Windley, B.F., Xiao, W.J., 2018. Ridge subduction and slab windows in the Central Asian Orogenic Belt: tectonic implications for the evolution of an accretionary orogen. Gondwana Res. 61, 73–87.
Xiao, W.J., Windley, B.F., Badarch, G., Sun, S., Li, J., Qin, K., Wang, Z., 2004. Palaeozoic accretionary and convergent tectonics of the southern Altaids: implications for the growth of Central Asia. J. Geol. Soc. 161, 339–342.
Xiao, W.J., Han, C.M., Yuan, C., Sun, M., Lin, S.F., Chen, H.L., Li, Z.L., Li, J.L., Sun, S., 2008. Middle Cambrian to Permian subduction-related accretionary orogenesis of northern Xinjiang, NW China: implications for the tectonic evolution of central Asia. J. Asian Earth Sci. 32, 102–117.
Xiao, W.J., Windley, B.F., Yuan, C., Sun, M., Han, C.M., Lin, S.F., Chen, H.L., Yan, Q.R., Liu, D.Y., Qin, K.Z., Li, J.L., Sun, S., 2009. Paleozoic multiple subduction–accretion processes of the southern Altaids. Am. J. Sci. 309, 221–270.
Xiao, W.J., Huang, B.C., Han, C.M., Sun, S., Li, J.L., 2010. A review of the western part of the Altaids: a key to understanding the architecture of accretionary orogens. Gondwana Res. 18, 253–273.
Xiao, W.J., Windley, B.F., Sun, S., Li, J.L., Huang, B.C., Han, C.M., Yuan, C., Sun, M., Chen, H.L., 2015. A Tale of amalgamation of three Permo-Triassic collage systems in central Asia: oroclines, sutures, and terminal accretion. Annu. Rev. Earth Planet Sci. 43, 477–507.
Xu, X.W., Jiang, N., Li, X.H., Qu, X., Yang, Y.H., Mao, Q., Wu, Q., Zhang, Y., Dong, L.H., 2013. Tectonic evolution of the east Junggar terrane: evidence from the Taheir tectonic window, Xinjiang, China. Gondwana Res. 24, 578–600.
Xu, Y.G., Wei, X., Luo, Z.Y., Liu, H.Q., Cao, J., 2014. The early Permian Tarim large igneous Province: main characteristics and a plume incubation model. Lithos 204, 20–35.
Yang, T.N., Li, J.Y., Liang, M.J., Wang, Y., 2015. Early Permian mantle-crust interaction in the south-central Altaids: high-temperature metamorphism, crustal partial melting, and mantle-derived magmatism. Gondwana Res. 28, 371–390.
Yuan, C., Sun, M., Xiao, W.J., Li, X.H., Chen, H.L., Lin, S.F., Xia, X.P., Long, X.P., 2007. Accretionary orogenesis of the Chinese Altai: insights from Paleozoic granitoids. Chem. Geol. 242, 22–39.
Zhang, C., Liu, D.D., Luo, Q., Liu, L.F., Zhang, Y.Z., Zhu, D.Y., Wang, P.F., Dai, Q.Q., 2018. An evolving tectonic environment of late carboniferous to early Permian granitic plutons in the Chinese Altai and eastern Junggar terranes, central Asian orogenic belt, NW China. J. Asian Earth Sci. 159, 185–208.
Zhang, C.L., Santosh, M., Zou, H.B., Xu, Y.G., Zhou, G., Dong, Y.G., Ding, R.F., Wang, H. Y., 2012. Revisiting the "Irtish tectonic belt": implications for the Paleozoic tectonic evolution of the Altai orogen. J. Asian Earth Sci. 52, 117–133.
Zhang, B., Zhang, J.J., Chang, Z.F., Wang, X.X., Cai, F.L., Lai, Q.Z., 2012. The Biluoxueshan transpressive deformation zone monitored by synkinematic plutons, around the Eastern Himalayan Syntaxis. Tectonophysics 574, 158–180.
Zhang, Z., Zhou, G., Kusky, T.M., Yan, S., Chen, B., Zhao, L., 2009. Late Paleozoic volcanic record of the Eastern Junggar terrane, Xinjiang, Northwestern China: major and trace element characteristics, Sr–Nd isotopic systematics and implications for tectonic evolution. Gondwana Res. 16, 201–215.
Zhang, Z.C., Yan, S.H., Chen, B.L., Zhou, G., He, Y.K., Chai, F.M., He, L.X., Wan, Y.S., 2006. SHRIMP zircon U-Pb dating for subduction-related granitic rocks in the northern part of east Jungaar, Xinjiang. Chin. Sci. Bull. 51, 952–962.
Zhuang, Y.X., 1994. The pressure-temperature-space-time (PTSt) evolution of metamorphism and development mechanism of the thermal-structural-gneiss domes in the Chinese Altaids. Acta Geol. Sin. 68, 35–47 in Chinese with the English abstract.